Quantifying soil loss with in-situ cosmogenic ^{10}Be and ^{14}C depth-profiles

Réka-H. Fülöp[a,b,c,*], Paul Bishop[b], Derek Fabel[b], Gordon T. Cook[c], Jeremy Everest[d], Christoph Schnabel[c], Alexandru T. Codilean[a], Sheng Xu[c]

[a]*School of Earth and Environmental Sciences, University of Wollongong, Wollongong NSW 2522, Australia*
[b]*School of Geographical and Earth Sciences, University of Glasgow, Glasgow G12 8QQ, Scotland UK*
[c]*Scottish Universities Environmental Research Centre (SUERC), East Kilbride G75 0QF, Scotland UK*
[d]*British Geological Survey, Edinburgh, EH9 3LA, Scotland UK*

Abstract

Conventional methods for the determination of past soil erosion provide only average rates of erosion of the sediment's source areas and are unable to determine the rate of at-a-site soil loss. In this study, we report in-situ produced cosmogenic ^{10}Be, and ^{14}C measurements from erratic boulders and two depth-profiles from Younger Dryas moraines in Scotland, and assess the extent to which these data allow the quantification of the amount and timing of site-specific Holocene soil erosion at these sites. The study focuses on two sites located on end moraines of the Loch Lomond Readvance (LLR): Wester Cameron and Inchie Farm, both near Glasgow. The site near Wester Cameron does not show any visible signs of soil disturbance and was selected in order to test (i) whether a cosmogenic nuclide depth profile in a sediment body of Holocene age can be reconstructed, and (ii) whether in situ ^{10}Be and ^{14}C yield concordant results. Field evidence suggests that the site at Inchie Farm has undergone soil erosion and this site was selected to explore whether the technique can be applied to determine the broad timing of soil loss. The results of the cosmogenic ^{10}Be and ^{14}C analyses at Wester Cameron confirm that the cosmogenic nuclide depth-profile to be expected from a sediment body of Holocene age can be reconstructed. Moreover, the agreement between the total cosmogenic ^{10}Be inventories in the erratics and the Wester Cameron soil/till samples indicate that there has been no erosion at the sample site since the deposition of the till/moraine. Further, the Wester Cameron depth profiles show minimal signs of homogenisation, as a result of bioturbation, and minimal cosmogenic nuclide inheritance from previous exposure periods. The results of the cosmogenic ^{10}Be and ^{14}C analyses at Inchie Farm show a clear departure from the zero-erosion cosmogenic nuclide depth

*Corresponding author
Email address: `rfulop@uow.edu.au` (Réka-H. Fülöp)

profiles, suggesting that the soil/till at this site has undergone erosion since its stabilisation. The LLR moraine at the Inchie Farm site is characterised by the presence of a sharp break in slope, suggesting that the missing soil material was removed instantaneously by an erosion event rather than slowly by continuous erosion. The results of numerical simulations carried out to constrain the magnitude and timing of this erosion event suggest that the event was relatively recent and relatively shallow, resulting in the removal of circa 20 - 50 cm of soil at a maximum of ~2000 years BP. Our analyses also show that the predicted magnitude and timing of the Inchie Farm erosion event are highly sensitive to the assumptions that are made about the background rate of continuous soil erosion at the site, the stabilisation age of the till, and the density of the sedimentary deposit. All three parameters can be independently determined a priori and so do not impede future applications to other localities. The results of the sensitivity analyses further show that the predicted erosion event magnitude and timing is very sensitive to the ^{14}C production rate used and to assumptions about the contribution of muons to the total production rate of this nuclide. Thus, advances in this regard need to be made for the method presented in this study to be applicable with confidence to scenarios similar to the one presented here.

Keywords: in-situ ^{14}C, in-situ ^{10}Be, cosmogenic depth-profile, soil erosion, Loch Lomond Readvance, Younger Dryas moraine

1. Introduction

The economic costs of soil erosion are clear (Pimentel et al., 1995; Montgomery, 2007), but despite the substantial agro-economic research in this field, many questions of a broader scientific importance have remained unanswered. It is not actually known, for example, whether human activity accelerates soil erosion (Trimble and Crosson, 2000; Fuchs, 2007), but it is nonetheless widely assumed that it does so by at least one order of magnitude (Walling and Webb, 1996; Hooke, 2000; Hewawasam et al., 2003; Wilkinson and McElroy, 2007). The problems associated with identifying human activity induced acceleration of soil erosion are twofold. First, it is uncertain whether studies of soil erosion based on historical data, decadal soil erosion plot data, and models such as RUSLE – that all point towards an acceleration of soil erosion due to human activity (e.g., Hooke, 2000; Wilkinson and McElroy, 2007; Montgomery, 2007) – are in fact capturing the variability of background (natural) erosion rates due to climate forcing, given that climatically driven perturbations can occur over the timescales that are pertinent to these short-term soil erosion studies (Daniels et al., 1987; Alford, 1992). Second, the mismatch between sediment yield data (Milliman et al., 1987) and long-term rates of sediment production (Clapp et al., 2000; Buechi et al., 2014) does not necessarily imply recently accelerated soil erosion rates given that, as shown by Clapp et al. (2000), elevated sediment yields can be the result of rivers reworking alluvial deposits and evacuating sediment deposited in earlier periods.

Despite the role of soils and soil erosion in the dyamics of the Earth's surface, current numerical models of long-term landscape evolution treat the former in a very simplistic way (Bishop, 2007; Tucker and Hancock, 2010). A better understanding of the controls on rates and depths of soil production and erosion (Bishop, 2007, and references therein) is needed for the improvement of these numerical models. The latter have played and play an important role in our understanding of the links and feedbacks between tectonics, climate, and surface processes, and improved models will enable us to go some way towards solving the so called 'chicken and egg' paradox posed by Molnar and England (1990) more than two decades ago and debated since (Willenbring and von Blanckenburg, 2010; Herman et al., 2013).

Furthermore, soil is an important component of the global carbon cycle (Lal, 2004). The removal of soil organic carbon by accelerated erosion could be contributing to the 740 Gt of carbon in the global mass of atmospheric CO_2, with emissions of 1 Gt of C/year (Lal, 2005) not just affecting the carbon stock but also carbon mineralization. Quantifying both soil erosion and soil age will contribute to the understanding of the complex nature of soil carbon storage and release dynamics (Harden et al., 1992).

Although age-controlled process-rates data related to soils are still sparse (Schaller et al., 2004), different dating techniques, such as radiocarbon (Wells et al., 1987; Trumbore, 1993; Anselmetti et al., 2007), U-Th series radionuclides (Cornu et al., 2009; Ma et al., 2010), OSL (Fuchs and Lang, 2001), and meteoric and in-situ produced cosmogenic nuclides (Barg et al., 1997; Small et al., 1999; Heimsath et al., 1997, 1999, 2000; McKean et al., 1993; Riebe et al., 2003; Wilkinson and Humphreys, 2005; Schaller et al., 2009, 2010), have been employed successfully. Of the aforementioned dating techniques, cosmogenic nuclide analysis is perhaps the most promising in terms of quantifying soil erosion, as (i) it enables the quantification of both catchment-wide and at-a-site erosion rates, and (ii) is sensitive over the millennial timescales relevant to both soil production and soil loss.

In this study, we report in-situ produced cosmogenic ^{10}Be, and ^{14}C measurements from erratic boulders and two depth-profiles from Younger Dryas moraines in Scotland, and assess the extent to which these data allow the quantification of the amount and timing of site-specific Holocene soil erosion at these sites. Similarly to other areas affected by Quaternary glaciations, most of Scotland's soils are formed on glacial till. Unlike in the case of soils that form by the in-situ weathering of the underlying bedrock, the age of soils formed on glacial till is quantifiable, as it is coeval with the age of till stabilisation. The latter is particularly important for this study, as the cosmogenic ^{10}Be and ^{14}C-based method presented here is based on the assumption that the age of soil formation is known.

2. Theoretical background

Different cosmogenic nuclides have different production pathways, and the production rates for these different production pathways attenuate differently with depth (Strack et al., 1994; Brown et al., 1995; Heisinger et al., 1997, 2002a,b). Thus, at least in theory, the depth-profiles of cosmogenic nuclides can provide more information on the processes that operate at the Earth's surface than a single nuclide concentration obtained from a surface sample (cf. Braucher et al., 2003; Kim and Englert, 2004; Schoenbohm et al., 2004). Given the vertical nature of soil processes, most studies involving soils and employing cosmogenic nuclides have used cosmogenic nuclide depth-profiles. For example, Brown et al. (1994) and Braucher et al. (1998) have used in-situ ^{10}Be depth-profiles in lateritic tropical soils to explain the formation of certain soil deposits. Phillips et al. (1998), using a model of soil burial by colluvium and bioturbation in combination with ^{21}Ne measurements in depth-profiles, were able to estimate inheritance-corrected exposure ages in stream terraces and an alluvial fan. Further, Schaller et al. (2003) combined ^{10}Be measurements in cover bed depth-profiles and river sediment in order to determine the effect of cover beds on catchment-wide erosion rate determinations.

The examples presented above are all based on the work of Anderson et al. (1996), who showed that a cosmogenic nuclide depth-profile in an alluvial deposit can be used to calculate the depositional age of that deposit by explicitly accounting for the inherited nuclide component. In short, Anderson et al.'s (1996) method works by reconstructing the cosmogenic nuclide depth-profile of the alluvial deposit and using the shift in this profile to estimate the amount of time elapsed since emplacement of that deposit. This principle, if inverted, can at least in theory be applied to quantifying at-a-site soil erosion events in soils formed on deposits of known age. If the age of the deposit is known independently (from, for example, absolute geochronology), the expected cosmogenic nuclide depth-profile in the sediment can be generated using that independently-known age and measured or assumed bulk densities. As in the case of Anderson et al. (1996), the measured nuclide concentration profile provides an estimate of inheritance. More importantly, the profile's total measured post-depositional nuclide inventory, whether that profile is perturbed or not, should match the total nuclide inventory estimated for a deposit of that age. Any shortfall in the measured total nuclide inventory compared to the total nuclide inventory predicted for the age of the deposit must reflect loss of nuclide, presumably by loss of the nuclide-bearing clasts, which are quartzose for the cosmogenic nuclides that are currently commonly measured, namely, ^{10}Be, ^{26}Al, ^{14}C and ^{21}Ne. Such quartz may conceivably be lost from the profile by lateral or vertical translocation within the soil/sediment, but it is likely that surface erosion is a more important mechanism for loss of nuclide-bearing quartz. For the simplest case of a profile that has not been perturbed by vertical movement of clasts, such surface erosion will truncate the top of the nuclide concentration profile. If the depth-profile of nuclide concentrations has been truncated by surface erosion and is also perturbed by vertical movement of clasts, the soil loss will notionally be revealed by a shortfall between the measured total inventory and the expected total inventory for the deposit's age and bulk density.

The degree to which surficial erosion of a sediment body of known age will be discernible in the cosmogenic nuclide depth-profiles depends on the timing of that erosion (e.g., ancient vs. recent) and its nature (e.g., continuous erosion vs. instantaneous erosional *events*), as well as on the age of the sediment body relative to the half-life and production rate of the cosmogenic nuclide in question. Depth-profiles of ^{10}Be (or ^{26}Al) in a Holocene sediment body, for example, do not record Holocene erosional events, whereas the depth-profile of in-situ ^{14}C in a similar sediment body that has been truncated by Late Holocene erosion is distinguishable from the profiles resulting from Middle Holocene events (Figure 1).

3. Study Area

The study was conducted at two sites: Wester Cameron Farm, near Glasgow, and Inchie Farm, near Lake of Menteith (Figure 2). Both sites are on Younger Dryas Loch Lomond Readvance (LLR) end-moraines. The Younger Dryas glacial readvance is well documented in Scotland (e.g., Sissons, 1967; Thorp, 1991; Golledge, 2010). Several published LLR moraine radiocarbon ages place a first order age constraint on the age of till deposition. In addition, the site at Wester Cameron is close to Croftamie, the well-studied LLR type-locality (Coope and Rose, 2008).

Scotland's landscape is dominated by glacial landforms that have been mostly preserved from the Last Glacial Maximum, which had maximum extent between ∼17 - 18 kyr (Stone et al., 1998). The LLR perturbation of this landscape started at around 13 kyr (Stone and Ballantyne, 2006) and peaked at the middle of the Younger Dryas, with a maximum mean annual temperature at sea level of 2°C (Ballantyne, 1984). The LLR was a short-lived (∼1.3 kyr) glacial incursion, with low erosive power and a still-debated ice thickness (Jack, 1877; Sissons, 1979; McIntyre and Howe, 2010). Radiocarbon dating indicates that LLR glaciers achieved their maximum extent after circa 12.8 kyr (Golledge et al., 2007) and the youngest set of end moraines were dated to around 11.6 kyr (Dugan, 2008) with in-situ ^{14}C. The LLR was followed by rapid deglaciation (Howe et al., 2002) mainly due to Scotland's climatic position (Lowell, 2000), with evidence for climatic amelioration before 10.5 kyr BP (Walker, 1995). The rapid recession is also supported by glaciotectonic structural evidence (Phillips et al., 2002). Localised ice stagnation might have occurred due to the glaciers' isolation related to their accumulation areas (Benn, 1992). The LLR was the last time that the Scottish highlands were occupied by glaciers (Golledge and Hubbard, 2005; Bradwell et al., 2008).

Prominent end moraines mark the limit of the LLR at several localities north of Glasgow, including our study sites (Figure 2; Evans et al., 2003). The Lake of Menteith moraine has been interpreted as a proglacially-folded and thrust moraine, with the suggestion that the LLR moraine at Wester Cameron may have the same origin (Evans and Wilson, 2006). The type section for the LLR, at Croftamie (Figure 2), demonstrates that the Loch Lomond glacier reached its maximum extent after 10,560 $\pm$ 160 ^{14}C yrs BP (11.9 - 12.7 cal kyr BP [2σ] - OxCal v.4.2, 2014) (Rose et al., 1989). There is evidence for continuous glaciomarine sedimentation after 10,350$\pm$125 ^{14}C yrs BP (11.7 - 12.6

cal kyr BP [2σ]- OxCal v.4.2, 2014) (Browne and Graham, 1981) suggesting a somewhat later deglaciation age (Gordon, 1982), in agreement with the recent findings of Palmer et al. (2010), placing the deglaciation closer to the Holocene. A radiocarbon age of 11,800 $\pm$ 170 ^{14}C yrs BP from a shell at the Lake of Menteith moraine (13.3 - 14.0 cal kyr BP [2σ]- OxCal v.4.2, 2014) records a Lateglacial Interstadial high sea level, suggesting that the LLR glacier advance occurred after this date (Sissons, 1967). However, most of the radiocarbon age determinations on shells (which in themselves are problematic due to the marine reservoir effect) were undertaken during the 1960s and 1970s, and have large uncertainties. To date, the uncertainties related to the LLR glaciers' central and eastern extensions remain unresolved (Golledge et al., 2008; Golledge, 2010).

The Wester Cameron Farm study site is located approximately 20 km northwest of Glasgow in the vicinity of Croftamie (56.01°N, 4.47 °W; Figure 2). The sampled end moraine is at an elevation of $\sim$168 m and shows no evident signs of disturbance: the study site is away from farm tracks, is not forested (i.e., undisturbed by forestry activities), and has a flat crest. The age of moraine emplacement was established by cosmogenic ^{10}Be exposure dating of two erratic boulders found on the moraine. Samples for cosmogenic nuclide depth-profile measurements were collected in contiguous 15 cm depth increments from a $\sim$2.5 m deep pit opened on the stable crest of the moraine. The Wester Cameron soil is a peaty podzol with a clear B horizon, and is capped by a $\sim$15 - 30 cm thick, well-drained, and not gullied peat layer. The presence of the capping peat layer suggests prolonged soil stability and lack of erosion (cf. Edwards and Whittington, 2001) and confirms our initial observations about the lack of recent soil disturbance at this site. To quantify the age of the peat layer, and therefore, the extent to which it perturbed the cosmogenic nuclide depth-profiles by shielding cosmic rays, eight samples were collected for radiocarbon dating from a 21 $\times$ 27 $\times$ 15 cm peat monolith taken from the top of the moraine.

The Inchie Farm study site is located approximately 23 km west-northwest of Stirling on the shore of Lake of Menteith (56.18°N, 4.27 °W; Figure 2). The pit for a cosmogenic nuclide depth-profile was excavated on the steep inner flank of the moraine ($\sim$50 m high), below a marked erosional break in slope. The objective was to analyse a depth-profile in an obviously disturbed and eroded site. No erratic boulders could be found on the moraine. Given that both the Loch Lomond and Lake of Menteith lobes are mapped as part of the LLR, we assume that the ^{10}Be exposure age obtained for Wester Cameron is also representative for Inchie Farm. This assumption is supported by the the close physical proximity between the two sites and the similarity in stratigraphy and soil development (Douglass and Bockheim, 2006). As at Wester Cameron, a $\sim$2.5 m deep pit was opened and samples for cosmogenic nuclide analyses were collected at contiguous 15 cm depth intervals.

Photographs of the moraines at the two sites and detailed stratigraphic descriptions of the sampled pits are provided as part of the online supplementary material.

4. Methods

4.1. Cosmogenic nuclide analyses

In-situ cosmogenic ^{10}Be and ^{14}C were analysed in a total of 35 samples. Of these, 33 were collected from two depth-profiles, and the remaining two from two erratic boulders. In-situ cosmogenic ^{10}Be was measured in all 35 samples, whereas in-situ ^{14}C was measured in only 15 of the 33 depth-profile samples.

4.1.1. In-situ ^{10}Be and ^{14}C measurements

Samples were wet-sieved and the 250 - 500 μm fraction was separated and labeled as CPA-F and LM-F, for Wester Cameron and Inchie Farm, respectively. The remaining sample material was separated in two size fractions: a coarse fraction (>2 mm) labeled CPA-P and LM-P, and one with grains between 0.5 mm - 2 mm labeled CPA-M and LM-M, respectively. These coarse (P) and medium (M) size fraction samples were then crushed using a jaw crusher, washed and dried. Quartz was isolated and cleaned following Kohl and Nishiizumi (1992). Prior to HF leaching, the bulk of aluminosilicates were removed using 85% pyro-phosphoric acid and a froth-flotation process using n-Dodecylamine surfactant.

Aliquots of 20 - 30 g from each sample were digested in concentrated HF, and Be was extracted using ion chromatography. The samples collected from Wester Cameron were prepared at the NERC Cosmogenic Isotope Analysis Facility at the Scottish Universities Environmental Research Centre (SUERC), and the samples collected from Inchie Farm were prepared at the Glasgow University Cosmogenic Isotope Analysis Facility, also based at SUERC. The two labs follow slightly different Be chemistry procedures, and these are described in detail in Wilson et al. (2008) and Child et al. (2000), respectively.

The ^{10}Be/^{9}Be ratios were measured at the SUERC 5MV NEC Pelletron Accelerator Mass Spectrometer (AMS) (Freeman et al., 2007). The measurements are described in detail in Maden et al. (2007), Schnabel et al. (2007), and Xu et al. (2010). ^{10}Be/^{9}Be ratios were normalised to the NIST SRM4325 standard, with a calibrated ^{10}Be/^{9}Be ratio of 3.06 $\times 10^{-11}$ (Middleton et al., 1993), 14% higher than the NIST certified value (^{10}Be/^{9}Be = 2.68 $\times 10^{-11}$). To make all subsequent calculations consistent with the updated ^{10}Be half-life of 1.387 $\pm$ 0.012 Myr (Chmeleff et al., 2010; Korschinek et al., 2010), the ^{10}Be concentrations reported here were re-normalised to the 2007 KNSTD standard (Nishiizumi et al., 2007). The ^{10}Be/^{9}Be ratios of the full chemistry procedural blanks prepared with the samples were 4.6 $\pm$ 1.1 $\times 10^{-15}$ (average of two blanks) and 5.6 $\pm$ 1.5 $\times 10^{-15}$ for Wester Cameron and Inchie Farm, respectively. Blank ratios were subtracted from the Be isotope ratios of the samples. Blank-corrected ^{10}Be/^{9}Be ratios of the samples ranged from 2.3 $\times 10^{-14}$ to 1.31 $\times 10^{-13}$ and 6.65 $\times 10^{-14}$ to 8.74 $\times 10^{-13}$ for Wester Cameron and Inchie Farm, respectively. Independent repeat measurements of AMS samples were combined as weighted means with the larger of the total statistical error or mean standard error. Final analytical error in concentrations (atoms.g^{-1} quartz) are derived from a quadrature sum of the standard mean error in AMS ratio, 2% for AMS standard reproducibility, and 2% in Be spike assay.

In-situ ^{14}C analyses were done on 5 g aliquots of purified quartz at the SUERC Radiocarbon Dating Laboratory. The system and extraction procedure used is described in detail by Naysmith et al. (2004), and Fülöp et al. (2010). Sample reproducibility, and the efficiency of the extraction system were tested using a Lake Bonneville shoreline surface quartz sample, which has been used as an internal standard at the University of Arizona (sample PP-4, Lifton et al., 2001) and the CRONUS-A laboratory inter-comparison sample (Jull et al., 2013). In-situ ^{14}C measurements of sample PP-4 yield an average of 4.09 $\pm$ 0.34 $\times$ 10^5 atoms.g^{-1} ($n = 9$), and those of sample CRONUS-A yield an average of 7.28 $\pm$ 0.24 $\times$ 10^5 atoms.g^{-1} ($n = 2$), both calculated following Hippe et al. (2013) and consistent with published values (Hippe et al., 2013; Jull et al., 2013).

Accelerator mass spectroscopy measurements were carried out at SUERC using both the 5MV NEC Pelletron AMS and the NEC 250 kV single stage AMS (Xu et al., 2004; Maden et al., 2007). The ^{14}C/^{13}C ratios were measured using oxalic acid standards (OxII) with a consensus value of 134.07 percent modern carbon (pMC). Uncertainty of individual sample measurement was derived from the χ^2-statistics test using statistical uncertainty of counting ^{14}C atoms and the scatter of ^{14}C/^{13}C ratios. Systematic uncertainties were assessed by secondary standards prepared from bulk barley mash (TIRI A) and individual Belfast cellulose (FIRI I) samples on a separate vacuum line, and from Icelandic doublespar (TIRI F) on the same vacuum line, with consensus values of 116.35 $\pm$ 0.0084 pMC, 57.10 $\pm$ 0.23, and 0.180 $\pm$ 0.006 pMC, respectively (Gulliksen and Scott, 1995; Scott, 2003). Thus, final analytical errors are derived from a quadrature sum of uncertainties of individual sample ^{14}C/^{13}C ratios and systematic uncertainties. Precision is limited by the statistical accuracy of counting, namely, 2% in ^{14}C/^{13}C ratios and is dependent on the carbon content and concentration of ^{14}C in the samples (Brown et al., 1984; Pigati et al., 2010).

AMS results were reduced according to the procedures set out by Hippe et al. (2013). Reported in-situ ^{14}C values were corrected using a combination of extraction blanks and full procedural blanks (shielded quartz), and graphitisation blanks. Bracketed blanks were used for the majority of samples. Where bracketed blanks were not available, the long-term (April 2009 – June 2010) average blank value of 5.89 $\pm$ 0.41 $\times$ 10^5 atoms ($n = 28$, $\pm 1\sigma$) was used for blank correction.

4.1.2. Depth-profile density measurements

Given that the attenuation of cosmic rays in a material depends on the density of that material (Lal, 1991), information on the later is key for accurately calculating the cosmogenic nuclide depth-profile in a deposit. Both pits were opened on moraines characterised by unsorted sediment consisting of clasts of varying sizes, and so standard methods for calculating density (cf. Balco and Stone, 2003) could not be applied. Instead, we used a terrestrial laser scanner (TLS) to map and calculate changes in the density of the till at both pits.

The sampled pit walls were scanned using a TLS before and after sampling so that a high-resolution DEM of the two surfaces can be constructed. During measurement, the instrument was held fixed on a tripod 2 - 3 metres from the scanned wall, yielding a 1 mm resolution point cloud. The scans were registered together, geo-referenced, and exported into an ASCII format. The point clouds were reduced to 25% of the initial size so that they can be handled by ArcGIS.

Using ArcGIS, the point clouds were triangulated and the resulting triangulated irregular networks (TIN) converted into regular grids. Triangulating first and then converting into a regular grid was preferred to directly interpolating the point cloud, as none of the interpolating techniques available in ArcGIS produced satisfactory results. The obtained regular grids (surfaces) were filtered to remove obvious artefacts (e.g., measuring tape present in some of the scans), and then used to calculate the volume of material removed by sampling (per individual pixel) by subtracting the pre-sampling grid from the post-sampling grid. Given that the TLS was held fixed on a tripod, a difference between the pre- and post-sampling grids only occurs for pixels where material was removed by sampling (i.e., for pixels were no material was sampled, the difference between the two surfaces will be zero). The per-pixel volume grids were then cut into 15 cm bands (as each sample was collected at contiguous 15 cm depth intervals) and the values summed for each band to yield the total volume removed from that band (= the total volume of each sample). Samples were weighed before and after drying in an oven and the sample masses and sample volumes were then used to calculate both an average dry and an average wet density for each 15 cm band.

4.2. Peat composition and radiocarbon analyses

The 21 $\times$ 27 $\times$ 15 cm peat monolith was collected from around one metre to the east of the cosmogenic nuclide depth-profile sample site at Wester Cameron Farm, and was located on the top of the moraine. The monolith sample was taken with a shovel and was wrapped in aluminium foil and kept in cold storage until sampling was undertaken. Prior to sampling, the monolith was split into two. One half was sampled for AMS radiocarbon analyses and the other half was sampled for particle size distribution, water content, organic matter content, and density. The latter analyses were aimed at characterising the peat and at assessing whether this has incorporated any moraine material.

Each of the eight AMS radiocarbon aliquots collected comprised of at least 40 g of sediment and was >1 cm thick. The aliquots were washed and all recognisable plant remains were removed. Peat is commonly used in radiocarbon dating, but complexity of biota can contribute to dating anomalies, usually there being discrepancies between the radiocarbon ages determined from the humin and humic fractions. In this study the humic acid (alkali soluble, acid insoluble) fraction was used for dating, and this can provide younger ages as it is mobile and may incorporate rootlets (Cook et al., 1998).

Following an acid-alkali-acid (AAA) pre-treatment, all aliquots were combusted and converted to CO_2 with CuO and silver wool, cryogenically purified, and then graphitised in the presence of Fe and Zn (Slota et al., 1987). Radiocarbon measurements were done at the SUERC AMS (Xu et al., 2004). We report radiocarbon dates in calibrated years before present, and these were calibrated with Oxcal v.4.2 (Bronk Ramsey and Lee, 2013) using the IntCal13 atmospheric calibration curve (Reimer et al., 2013) and a bayesian framework.

4.3. Depth-profile modelling

The accumulation of cosmogenic nuclides in a mineral grain buried beneath an eroding or non-eroding surface is accurately described by the following equation (Niedermann, 2002):

$$N(z,t) = N(z,0)e^{-\lambda t} + \\ + \sum_{i=4}^{4} \frac{P(0)_i}{\lambda + \rho\epsilon/\Lambda_i} e^{-\frac{\rho(z_p+\epsilon t)}{\Lambda_i}} \left(1 - e^{-(\lambda+\rho\epsilon/\Lambda_i)t}\right) \quad (1)$$

where $N(z,t)$ is the nuclide concentration (atoms.g^{-1}) as a function of depth below the surface, and time; λ is the decay constant of a radionuclide; $P(0)_i$ and Λ_i are the surface production rate (atoms.g^{-1}.yr^{-1}) and mean cosmic ray attenuation length (g.cm^{-2}) for the different production pathways; ρ is the density of the target material (g.cm^{-3}); t is the time since exposure to cosmic radiation (yr); ϵ is the erosion rate (cm.yr^{-1}); and z_p is the present burial depth (cm).

We use equation (1) to calculate the reference (*zero-erosion*) cosmogenic nuclide depth-profiles at our two study sites, and to model the evolution through time of the ^{10}Be and ^{14}C concentrations in the Inchie Farm depth-profile samples. The formulation in equation (1) allows for explicitly accounting for production of cosmogenic nuclides by muons. The calculations presented here account for production of cosmogenic nuclides through high-energy neutron spallation, negative muon capture, and fast muon induced bremsstrahlung, using the exponentials provided in Granger and Smith (2000) and Granger and Muzikar (2001). For ^{10}Be we use the sea-level, high-latitude (SLHL) high-energy neutron spallation production rate of 4.49 $\pm$ 0.39 atoms.g^{-1}.yr^{-1} (Stone, 2000; Balco et al., 2008), and the SLHL production rates for muons provided in Kubik et al. (2009) and based on Heisinger et al. (2002a,b), namely, 0.097 $\pm$ 0.007 atoms.g^{-1}.yr^{-1} for slow muons, and 0.085 $\pm$ 0.012 atoms.g^{-1}.yr^{-1} for fast muons, respectively. All of the above ^{10}Be production rates are compatible with the updated ^{10}Be half-life of 1.387 $\pm$ 0.012 Myr (Chmeleff et al., 2010; Korschinek et al., 2010). For ^{14}C we use the SLHL spallation production rate of 12.29 $\pm$ 0.99 atoms.g^{-1}.yr^{-1} (Hippe et al., 2012), and the SLHL production rates for muons provided in Heisinger et al. (2002a,b): 3.34 $\pm$ 0.27 atoms.g^{-1}.yr^{-1} for slow muons, and 0.44 $\pm$ 0.25 atoms.g^{-1}.yr^{-1} for fast muons, respectively. Our choice of ^{10}Be SLHL spallation production rate is somewhat higher than the recently recalculated value of 3.94 $\pm$ 0.20 atoms.g^{-1}.yr^{-1} (Heyman, 2014), albeit the two overlap at 1σ. Nevertheless, we use 4.49 $\pm$ 0.39 atoms.g^{-1}.yr^{-1} to be consistent with previous studies employing the ^{10}Be and ^{14}C pair (e.g., Hippe et al., 2012). We note that using the recalculated value will not change any of the results in a detectable way.

We construct a numerical model that works as follows. After stabilisation of the moraine, ^{10}Be and ^{14}C start accumulating in the sediment body, against a continuous (background) erosion rate. At a given moment in time (between moraine stabilisation and the present), a given thickness of soil is instantaneously removed from the surface of the sediment body by an erosional event, truncating the ^{10}Be and ^{14}C depth-profiles. Following this erosional event, cosmogenic ^{10}Be and ^{14}C continue to accumulate against the same or a different background erosion rate.

For any cosmogenic nuclide depth-profile corresponding to a single erosional event with a given timing and magnitude, one can minimise the difference between the measured ^{10}Be and ^{14}C depth-profiles and those predicted by the model, and therefore find the solution that best fits the data. However, given that the measured ^{10}Be and ^{14}C concentrations have an associated uncertainty, more than one erosional event timing and magnitude pair will provide a reasonable fit to the data. Under these circumstances the statistically most likely model solution can be obtained by minimising the chi-square (χ^2) statistic, given by (Bevington and Robinson, 2003):

$$\chi^2 = \sum \left(\frac{N_{\text{Measured}} - N_{\text{Modelled}}}{\sigma N_{\text{Measured}}} \right)^2 \tag{2}$$

where N_{Measured} and N_{Modelled} are the measured and modelled ^{10}Be and ^{14}C concentrations in each sample, respectively, and $\sigma N_{\text{Measured}}$ is the uncertainty in the measured ^{10}Be and ^{14}C concentrations. The χ^2 approach has been successfully applied to quantifying the depositional ages of eroding alluvial terraces (Siame et al., 2004; Hein et al., 2009; Braucher et al., 2009; Guralnik et al., 2010; Hidy et al., 2010) and of eroding moraines (Schaller et al., 2009).

When used as a goodness-of-fit indicator, χ^2 is reduced by dividing by the degrees of freedom given as $N_s - m$, where N_s is the number of measurements and m is the number of model parameters (Bevington and Robinson, 2003). If the modelled cosmogenic nuclide depth-profile is a good fit to the data, the reduced χ^2 (χ^2_{red}) should approach unity ($\chi^2_{red} = 1$). Values that are large or < 1 indicate that the modelled cosmogenic nuclide depth-profile is not appropriate at describing the measured concentrations (Bevington and Robinson, 2003). Given that the ^{10}Be and ^{14}C depth-profiles are independent of each other, separate χ^2_{red} maps can be produced for each nuclide and the intersection of the two will constrain the erosional event timing and magnitude pair that best fits the two datasets.

The model was implemented in the R statistical language (R Core Team, 2014) and model results are provided as contoured maps of χ^2_{red} values obtained for the full range of erosional event timing and magnitude pairs. The timing-magnitude pair with the lowest χ^2_{red} (if not < 1) is considered to be the one that is most likely to explain the data. The 68% (1σ level) confidence interval around the best-fit parameter combination is given by $\chi^2_{red}(min) + 1$ (Bevington and

Robinson, 2003).

5. Results and Discussion

The results of the cosmogenic ^{10}Be analyses in the Wester Cameron erratic boulders are shown in Table 1, and the results of the radiocarbon determinations in the Wester Cameron peat are shown in Table 2. Results of the ^{10}Be and ^{14}C analyses in the Wester Cameron and Inchie Farm depth-profiles are shown in Tables 3 and 4, respectively, and in Figure 3.

5.1. Wester Cameron

5.1.1. Age of till stabilisation

The ^{10}Be analyses on the two erratic boulders at Wester Cameron yield an average exposure age of 10.5 ± 1.0 kyr (Table 1), slightly younger than the published radiocarbon ages for the LLR maximum ice extent (see above). Stratigraphic analyses at both study sites (see online supplementary material) indicate complex glacio-fluvial processes associated with ice margins (Gerrard, 1992), and there are uncertainties associated with the form of deposition and exact timing of the LLR. However, as argued earlier, the similarity in stratigraphy and soil development (Douglass and Bockheim, 2006) and the close physical proximity between the two sites indicate that the cosmogenic ^{10}Be exposure age determined at Western Cameron is likely to be also representative of the moraine at Inchie Farm. Therefore, we take 10.5 kyr to be the age of till stabilisation at both study sites, and use this value in all further calculations. Neither the type of till formation nor lithology affect the cosmogenic ^{10}Be and ^{14}C depth-profiles. The attenuation with depth of cosmic rays, and therefore the shape of the depth-profiles, is mainly a function of the density of the penetrated material. The latter has been thoroughly characterised at both sample sites.

5.1.2. Duration of peat cover

Blanket peats formed throughout the Holocene due to the cool and wet temperate climate, and occupy an extensive area of Scotland. Blanked peat is formed as a result of slow decomposition of organic matter, mainly sphagnum moss (Borren et al., 2004). The peat cover at Wester Cameron is relatively shallow (15 - 30 cm) and has an angulated mineral rich base. Total organic matter content, estimated as loss-on-ignition at 500°C (Gale and Hoare, 1991), showed a linear decrease with depth, indicating that the growth of the peat layer was continuous.

The obtained radiocarbon ages (Table 2) are stratigraphically coherent, except for the reversal of samples 21601 and 21600. These two samples were collected from the contact zone between the peat and the underlying mineral substrate, and we attribute the reversal to the introduction of younger carbon by groundwater percolating along the relatively impermeable surface at the base of the peat. Sample 19861 is modern. Accepting the radiocarbon determinations for the rest of the samples as correct implies a basal age for the peat of

1400-2000 radiocarbon years, depending on whether the top of the peat or the root zone (which returned the modern age) or the present ground surface are taken to be the reference point. Based on this basal age determination, peat formation started at between 500 - 2157 years ago. Independent of whether the minimum or maximum calibrated ages are used or whether the root zone or ground surface are used as a reference point, the Wester Cameron peat started forming at a maximum of ∼2000 years BP. This relatively young age combined with a measured bulk density of 0.5 - 0.9 g.cm^{-3} indicates that the peat cover at Wester Cameron did not shield substantially the soil from cosmic rays, and so did not have a substantial effect on the accumulated cosmogenic nuclide concentrations. Notwithstanding, the shielding effect of the peat layer on nuclide production is fully accounted for in all further calculations.

5.1.3. Depth-profile form and grain size differences

The cosmogenic nuclide depth-profiles show declining ^{10}Be and ^{14}C concentrations with depth (Figures 3A & 3B). There is an indication of homogenisation of the upper 70 cm, that exhibit similar concentrations. The process has mixed both the coarsest and finest grain sizes and has either acted throughout the last ∼10.5 kyrs or is sufficiently recent to homogenise ∼10.5 kyr worth of cosmogenic nuclide in-growth at the two depths. A range of mechanisms could be responsible for such mixing, including bioturbation by large soil fauna and/or large flora (e.g., by tree fall and root throw), and perhaps cryoturbation, all restricted to the top 50 - 70 cm of the till and presumably pre-dating the growth of the peat that caps the moraine. Cryoturbation is unlikely for at least two reasons: (1) no structures were evident in the till sediments indicative of cryoturbation at any depth in the moraine; and (2) if cryoturbation did occur, this would have happened most likely immediately after the LLR and is unlikely in later Holocene climates at the moraine's elevation. If the shallowest two samples had been cryoturbated in the early Holocene, subsequent (middle and late Holocene) acquisition of cosmogenic nuclides would have restored the exponential depth-profile.

On soils that have not been disturbed by vertical movement and homogenisation of material, erosion removes the high cosmogenic nuclide concentration surface material, reducing the total cosmogenic nuclide inventory while not affecting the exponential shape of the depth-profile. Homogenisation of the upper part of a cosmogenic nuclide depth-profile, either by bioturbation or cryoturbation, will result in migration of low nuclide concentration sediment upward. Erosion of a homogenised soil layer, therefore, creates a mismatch between the integral of the concentration in the homogenised layer and the integral of the exponential *zero-erosion* cosmogenic nuclide depth-profile (cf. Perg et al., 2001). To test whether the surface of the soil was eroded prior to the formation of the peat cover, the total cosmogenic ^{10}Be inventory in the Wester Cameron pit was calculated by integrating the curve obtained by joining the ^{10}Be concentrations measured in the 0.25 - 0.5 mm size fraction (cf. Hidy et al., 2010) and the one obtained by integrating the curve defined by the *zero-erosion* cosmogenic ^{10}Be depth-profile (Figures 3A & 3B). The difference between the two inventories is

10%. This difference is similar to the uncertainty of the *zero-erosion* depth-profile, suggesting that the two inventories are essentially identical, suggesting in turn that the sediment at the Western Cameron site has not been eroded since its stabilisation.

There is generally little differentiation in ^{10}Be concentration by grain-size, and in the two cases where this is observed (at 97 cm and 142 cm sample depths) the coarser fraction has the lower concentration. This difference in ^{10}Be concentration between the different grain-sizes could simply be due to the fact that the coarser fraction amalgamates substantially fewer individual clasts than the finer fraction (i.e., $\sim$10 individual clasts in the coarser fraction vs. $\sim 10^5$ sand grains in the finer fraction), and so may easily under- or over-estimate the 'true' mean ^{10}Be concentration (cf. Hidy et al., 2010).

5.1.4. Cosmogenic nuclide inheritance

Glacial settings are susceptible to the issue of inheritance in exposure dating (Briner and Swanson, 1998; Fabel et al., 2002; Bierman, 2007). Such inheritance may arise, for example, from clasts dropping onto the ice surface from the exposed valley side above the ice, or, probably more likely, in situations where an ice mass erodes and deposits material that has been exposed to cosmic radiation prior to that glacial episode, which does not erode sufficient depth of material ($\sim$2 m) to be then eroding cosmogenic nuclide-free material (Stroeven et al., 2002; Bierman and Nichols, 2004). This situation commonly arises when cold-based ice achieves minimal erosion because it is frozen to the bed (Staiger et al., 2005). There is little evidence in the Wester Cameron LLR moraine depth-profile of nuclide inheritance, with all but one of the measured ^{10}Be concentrations (i.e., apart from the top bioturbated sample at 70 cm depth) lying either side of, and overlapping with, the calculated *zero-erosion* depth-profiles, within the uncertainties of that calculated profile and the measured concentrations. The only possible exception is the medium-sized fraction of the deepest sample (225-240 cm), which returned a ^{10}Be nuclide concentrations slightly greater than that predicted by the calculated depth-profile for a $\sim$10.5 kyr-old moraine with the densities of the Wester Cameron till (Figure 3B2). The ^{10}Be concentrations of the coarse- and fine-grained fractions of that deepest sample lie squarely within the uncertainties of the calculated depth-profile and the nuclide concentration measured in the medium-sized fraction is indistinguishable at 1σ from the nuclide concentrations measured in those other two size fractions. It is therefore reasonable to conclude that the clasts record minimal inherited nuclide concentration. It is important to remember that even though the deepest clasts have ^{10}Be concentrations of the order of 10^3 - 10^4 atoms.g^{-1} (corresponding to <2 kyr of exposure for a production rate of $\sim$5 atoms.g^{-1}.yr^{-1} at the ground surface), the calculated depth-profile shows that that concentration will accumulate over 10.5 kyr at that depth in clasts with a minimal amount of inheritance (equivalent to a maximum of $\sim$800 years of exposure) in a sedimentary body with the measured densities of the Wester Cameron moraine.

The low nuclide inheritance in clasts in the Wester Cameron LLR moraine is likely to reflect several factors. Firstly, the Younger Dryas Loch Lomond valley glacier was not cold-based and hence was able to erode its bed and remove much of the upper ∼2 m of ground surface that was exposed during the preceding ice-free Windermere Interstadial. Secondly, the Windermere Interstadial was of relatively short duration, meaning that the clasts in the LLR moraine sampled here had relatively short duration of exposure to cosmic radiation, hence minimising the in-growth of cosmogenic ^{10}Be prior to the LLR. Thirdly, and conversely, the LLR was itself of relatively short duration, making it more likely that boulders with nuclide inheritance would have been retained within the system and be available for sampling. Departures of the measured LLR till ^{10}Be depth-profile from the *zero-erosion* cosmogenic nuclide depth-profiles for a ∼10.5 kyr-old Wester Cameron-type till are minor, pointing to a relatively simple post-depositional history of acquisition of ^{10}Be. The simple exposure history of the soil/till at the Wester Cameron site is also confirmed by the insignificant departures of the ^{14}C results from the *zero-erosion* cosmogenic nuclide depth-profiles (Figures 3C).

5.2. Inchie Farm

5.2.1. Depth-profile characteristics

Unlike the results for the Wester Cameron site, the ^{10}Be and ^{14}C concentrations at the Inchie Farm site show a clear departure from the *zero-erosion* cosmogenic nuclide depth-profiles obtained for an exposure duration of 10.5 kyr (Figures 3E & 3F). The measured profiles lie to the left of the *zero-erosion* depth-profiles, indicating that either (1) the soil/till at this site has undergone erosion sufficiently recently since its emplacement that has not permitted the full 'uneroded' depth-profile to be re-established; or (2) the soil/till was shielded by a layer of peat that has been subsequently removed; or (3) there was no erosion but the age of soil/till stabilisation is younger than 10.5 kyr. The possibility of a peat cover can be easily excluded. The relatively low density of peat means that a peat cover of at least 60 cm is needed for an exposure duration of at least 10.5 kyr, to explain the departure from the *zero-erosion* cosmogenic nuclide depth-profiles observed at Inchie Farm. Moreover, the presence of a cover that has been subsequently removed is tantamount to (1). In the absence of erosion, an exposure duration of 7.5 kyr is necessary to reproduce the ^{10}Be and ^{14}C concentrations obtained at Inchie Farm. This age is substantially younger than the deglaciation ages recorded in Scotland (Benn and Lukas, 2006). Therefore, the most likely explanation for the obtained ^{10}Be and ^{14}C concentrations is that the soil/till at this site has undergone erosion sufficiently recently since its emplacement.

5.2.2. Magnitude and timing of erosion

The LLR moraine at the Inchie Farm site is characterised by a sharp apparently erosional break-in-slope on its inner flank (see online supplementary material for photograph), suggesting that the missing soil material was removed instantaneously in a short erosional event. Had the moraine been subjected to slow continuous erosion, rather than a virtually instantaneous erosional event, the break-in-slope would very likely have been rounded off and erased. The shape of the Inchie Farm moraine suggests some post-glacial stabilisation, since fresh LLR moraines tend to be triangular in cross section, and sharp-crested moraines will tend to stabilise to being shorter, as material moves from the moraine's crest to its flanks and toe (Anderson and Humphrey, 1989; Hallet and Putkonen, 1994; O'Neal, 2006; Putkonen et al., 2007; Pelletier, 2008). This stabilisation most likely occurs relatively soon after deglaciation and hence will not affect the cosmogenic ^{10}Be and ^{14}C results. And even if the post-glacial stabilisation is not 'instantaneous', it will presumably slow with time as the 'adjusted' form is approached.

We constrain the likely magnitude and timing of the erosional event using a bootstrapping approach based on equations (1) and (2), as described in the methods section. The analysis was carried out at first for each cosmogenic nuclide separately. For each nuclide, an almost infinite combination of erosional event magnitude and timing pairs produce fits with low χ^2_{red} values suggesting that ^{10}Be or ^{14}C on their own cannot constrain the magnitude and timing of a Holocene soil erosional event (Figure 4A). However, the χ^2_{red} contour plots obtained for the two nuclides are markedly different and when used together, ^{10}Be and ^{14}C will substantially narrow the range of erosional event magnitude and timing pairs that provide good fits to the data. Combining the two nuclides and performing the analysis using both ^{10}Be and ^{14}C depth-profiles together yields a narrower set of likely erosional event magnitude-timing pairs (Figure 4B). The lowest χ^2_{red} values ($\sim$1.5) are obtained for erosional events that occurred between 0 and 500 years ago and resulted in the instantaneous removal of between 30 to 35 cm of soil. Considering the 68% confidence interval (Figure 4B) (min $\chi^2_{red} + 1 = 2.5$), the results of our analysis indicate that the erosional event is very likely to be relatively recent ($<\sim$ 2000 years) and removed 20 - 50 cm of soil.

The results of our analyses suggest that the erosion event at Inchie Farm occurred in the last 1.5 kyr, with a best fit at 300 years B.P. Given that we only have one site, and therefore have only one estimate of the timing of the erosion event that removed the soil from this site, we can only speculate as to what the geomorphological meaning of this erosion event timing estimate is, if at all there is one. Studies employing a range of tools, including pollen, potassium, magnetic susceptibility, and radiocarbon analyses, have observed throughout Scotland's lakes, increases in sedimentation attributed to agricultural activity during the mid Holocene at 5, 4, 3, 1.5, and in some cases also at 0.3 kyr B.P. (Edwards and Whittington, 2001). In the 18th century, grain production in Scotland has increased following the independence war and the Union of Scotland and England 1707 Agriculture Progress Regulation Act. This century has also seen increases in deforestation as sheep grazing pressure increased with wool production becoming an important part of the economy (Smout and Fenton, 1965). This intensification of agriculture coupled with deforestation in 18th century Scotland could potentially be one explanation for the recent (0 to 500 years B.P.) timing of the erosion event obtained at Inchie Farm. Taking into account the uncertainty associated with our erosion event timing estimate, however, the loss of soil at Inchie Farm could also be linked to the advent of iron tools at around 500 B.C. (Barrett, 1981).

5.3. Sensitivity analysis

5.3.1. Non-zero continuous background erosion rate

Our analyses so far have assumed no (or negligible) continuous soil erosion but the possibility that the LLR moraine at Inchie Farm experienced continuous erosion cannot be completely ruled out. We repeat our analyses for continuous background erosion rates ranging between 5 and 100 mm.kyr^{-1} (Figure 5A). Continuous erosion rates of up to 10 mm.kyr^{-1} yield χ^2_{red} contour plots that are almost identical to that obtained when assuming a zero background erosion rate (Figure 5A1 and A2, and Figure 4A) suggesting that continuous erosion rates < 10 mm.kyr^{-1} will not affect the ^{10}Be and ^{14}C depth-profiles sufficiently to perturb the erosional event 'signal', albeit the lowest χ^2_{red} values are obtained for shallower events.

As for the > 10 mm.kyr^{-1} case, low χ^2_{red} values are obtained for recent and shallow erosional events when assuming a continuous erosion rate of 20 mm.kyr^{-1}. However, the ^{10}Be and ^{14}C depth-profiles are also equally well fitted by any erosional event older than 10 kyrs BP (Figure 5A3). For continuous erosion rates > 20 mm.kyr^{-1}, the ^{10}Be and ^{14}C depth-profiles are perturbed sufficiently such that no erosional event magnitude and timing pair provides a reasonable fit to the measured ^{10}Be and ^{14}C data. The fact that for continuous background erosion rates > 20 mm.kyr^{-1}, (i) the modelled ^{10}Be and ^{14}C depth-profiles poorly fit the data, and (ii) these fits have lower χ^2_{red} values than those obtained for the same rates but assuming no erosional events (Figure 5B), suggest that a continuous erosion alone (i.e. without an erosional event) is not sufficient to explain our ^{10}Be and ^{14}C data, and that these data are best explained by a combination of a discrete erosional event superimposed on a zero or relatively low (< 20 mm.kyr^{-1}) continuous background erosion rate.

The sensitivity analyses clearly show that for the magnitude and timing of an erosional event to be determined with confidence, the continuous background erosion rate should first be constrained. The latter can be achieved by measuring cosmogenic nuclide depth-profiles on those parts of the same moraine that do not show obvious signs of erosion (e.g., the stable crest of the moraine). Alternatively, erosion rates estimated elsewhere may be assumed to apply. The relatively few studies of soil erosion rates in Scotland generally report negligible or relatively low rates. For example, Kirkbride and Reeves (1993) found no erosion occurring on grasslands and Duck and McManus (1987) used reservoir sedimentation over periods of 35 - 121 years to calculate erosion rates of 2.1 - 52 t.km^2.yr^{-1}, equivalent to 1.2 - 28 mm.kyr^{-1}, at Angus, a site only two hours drive from Inchie Farm.

5.3.2. Age of till stabilisation

All model results presented so far were obtained taking the Wester Cameron erratic boulder's mean ^{10}Be exposure age of 10.5 kyr to be the age of till stabilisation at both Wester Cameron and Inchie Farm. However, as mentioned above, the timing of the LLR has been dated using radiocarbon measurements in samples from various locations including one collected from the vicinity of the Inchie Farm sample site (see Golledge et al. 2007 for a list of LLR radiocarbon ages). This latter sample was a marine shell found below the till deposit and yielded a radiocarbon age of 11.8 ± 0.17 ^{14}C kyr (Sissons, 1967), calibrated to ∼13.5 kyr BP using OxCal v.4.2. Gordon (1982) has argued that this age, being measured in marine shells, has likely been affected by the reservoir and hard-water effects (Heier Nielsen et al., 1995; Ascough et al., 2009). Moreover, there will also be a time lag between moraine formation and the radiocarbon age, unless the age is measured on the remains of a living organism buried during moraine formation (Lowell et al., 1990). Thus, it is likely that the mean ^{10}Be exposure age obtained at Wester Cameron is closer to the true age of till stabilisation at Inchie Farm than the radiocarbon age of ∼13.5 kyr BP. Nonetheless the effect of an older till stabilisation age on the predicted erosional event magnitude and timing pair is explored in Figure 6.

Assuming 13.5 kyr BP as the age of till stabilisation predicts an erosional event that is deeper and occurs somewhat earlier than the one obtained for 10.5 kyr (Figure 4B and Figure 6C). For each 1 kyr increase in the age of till stabilisation, the model predicts an increase of ∼10 cm in the depth of the erosional event and an increase of ∼300 years in the timing of the event (Figure 6). Although the changes shown in Figure 6 are not as dramatic as those obtained when considering a non-zero continuous background erosion rate (Figure 5), the results highlight the importance of accurately constraining the age of deposition if the magnitude and timing of the erosional event are to be reliably determined.

5.3.3. Density of the sediment

The density of till at both the Wester Cameron and Inchie Farm sites was determined at high resolution as described above. However, the density of glacial deposits is highly variable both from deposit to deposit and within an individual profile, and so a sensitivity analysis provides useful insights regarding future applications of this method to sites where such high-resolution data on till density are not available. For the purposes of the sensitivity analysis, till/soil density was allowed to vary at 0.1 g.cm^{-3} increments between 1.5 g.cm^{-3} and 2.4 g.cm^{-3}, the range typically quoted in the literature for glacial deposits (Fausey et al., 2000; Staiger et al., 2006). Although the density of a sedimentary deposit can also vary through time (cf. Rodés et al., 2011), this temporal variation is likely to be relatively insignificant in glacial deposits when compared to the spatial variation (i.e., between deposits) or the variation within a profile, and so such temporal variation is not considered here.

The results of the sensitivity analysis are shown in Figure 7, and illustrate that while there is no straight-forward relationship between the density of the sedimentary deposit and the predicted best-fit erosional event timing, although higher densities seem to yield older events, the former determines the obtained best-fit erosional event magnitude in both a predictable (the higher the density the shallower the best-fit erosional event) and substantial way (∼30 cm depth difference for a density range of 1 g.cm^{-3}). The two plots in Figure 7 should not be viewed in isolation, however. The lack of correlation between erosional event timing and material density, and the apparent negative correlation between erosional event magnitude and material density is simply a reflection of the exponential decrease of cosmogenic nuclide production rates with depth. In the case of soil profile truncation, on average, the amount of material removed by an erosional event will matter more than how far back in time the erosion event had occurred. In light of the above, for the method presented in this study to be applicable successfully to other sites, data on the density of the sedimentary deposit must be obtained a priori.

5.3.4. In-situ ^{14}C production rate

The results of age or denudation rate calculations involving cosmogenic nuclides depend highly on the sea level high latitude (SLHL) production rates that are used. The quality (or *accuracy*) of these production rates depend on (i) the quality of the calibration data sets, and (ii) the quality of the altitude/latitude scaling schemes used to calculate the production rates (Balco et al., 2008; Dunai, 2010). Calibration data sets represent cosmogenic nuclide concentration measurements at sites that have undergone negligible denudation and have ages that have been independently determined (see Balco et al. 2008 and Lifton et al. 2005, 2008 for a list of calibration sites used for ^{10}Be and ^{14}C). As the calibration site ages have associated uncertainties, these propagate into local cosmogenic nuclide production rates. Moreover, all calibration-site-specific local cosmogenic nuclide production rates are standardised to sea level and high latitude using one of the many altitude/latitude scaling schemes (e.g., Balco et al., 2008; Lifton et al., 2014). Each of these have an uncertainty. It is difficult to calculate the uncertainties of the currently used SLHL production rates but Balco et al. (2008) estimated that the 1σ uncertainty introduced by empirical scaling schemes may be as large as 10%. In short, although the currently used SLHL production rates for ^{10}Be and ^{14}C have quoted uncertainties, the true absolute uncertainties are unknown. The issues described above are especially pertinent to in-situ ^{14}C, as the SLHL production rate of this cosmogenic isotope is the least well constrained (cf. Dunai, 2010).

To assess the effect that these production rate uncertainties have on our results, the SLHL production rate of in-situ ^{14}C was varied by $\pm$ 10% (Figure 8A1 and A2). Further, we have also varied the contribution of high-energy neutron spallation to the total ^{14}C SLHL production rate from 83% (Heisinger et al., 2002a,b) to 90% (Figure 8B1) and to 100 % (Figure 8B2). Our results show that the predicted magnitude and timing of the erosional event are very sensitive to the ^{14}C SLHL production rate used and to assumptions about the contribution of muons to the total production rate of this nuclide. Thus, successful future applications of the method presented here are demand an improvement of our understanding of ^{14}C SLHL production rates and production systematics.

6. Conclusions

In this study we explore the extent to which in-situ cosmogenic ^{10}Be and ^{14}C depth-profiles can be used to quantify the magnitude and timing of site-specific erosional events over Holocene timescales on soils/sediments of known age. We focus on two sites located on end-moraines of the Loch Lomond Readvance in Scotland: Wester Cameron and Inchie Farm near Glasgow. Conclusions from the data and the results of the numerical simulations can be divided into two broad categories: (i) those concerning the amount and timing of erosion at both sites and (ii) those concerning the broader implications of the sensitivity analyses.

The conclusions concerning the amount and timing of soil erosion at the Wester Cameron and Inchie Farm sites are as follows:

(a) The results of the in-situ cosmogenic ^{10}Be and ^{14}C analyses in the Wester Cameron site samples confirm that the cosmogenic nuclide depth-profile to be expected from a sediment body of Holocene age can be reconstructed. Moreover, the agreement between the total cosmogenic ^{10}Be inventories in the erratics and the Wester Cameron soil/till samples indicate that there has been no erosion at the sample site since the deposition of the till/moraine. Further, the Wester Cameron depth-profiles show minimal signs of homogenisation, as a result of bioturbation, and minimal cosmogenic nuclide inheritance from previous exposure periods.

(b) The results of the in-situ cosmogenic ^{10}Be and ^{14}C analyses in the Inchie Farm site samples show a clear departure from the *zero-erosion* cosmogenic nuclide depth-profiles suggesting that the soil/till at this site has undergone erosion since its emplacement. The LLR moraine at the Inchie Farm site is characterised by the presence of a sharp break in slope upslope of the sampled depth-profile, suggesting that the missing soil material was removed instantaneously by an erosional event rather than by slow continuous erosion. The numerical analysis carried out to constrain the magnitude and timing of this erosion event suggests that this event was relatively recent and relatively shallow, resulting in the removal of circa 20 - 50 cm of soil at a maximum of $\sim$2000 years BP.

The conclusions concerning the broader implications of the sensitivity analyses are as follows:

(a) The results of the sensitivity analyses show that the predicted magnitude and timing of the Inchie Farm erosion event are highly sensitive to (i) assumptions about the background rate of continuous soil erosion at the site and (ii) the stabilisation age of the till. The results further indicate that the density of the sedimentary deposit (iii) will also affect the magnitude and timing of the predicted erosional event. All three parameters can be independently determined a priori and so despite the fact that the method presented here is sensitive to variations in these parameters, they do not impede future applications of the method.

(b) The results of the sensitivity analyses also show that the predicted magnitude and timing of the erosional event are very sensitive to the in-situ cosmogenic ^{14}C SLHL production rate used and to assumptions about the contribution of muons to the total production rate of this nuclide. Given that the production systematics of *in situ* ^{14}C are less well understood than those of other more routinely used cosmogenic nuclides, advances in this regard need to be made for the method presented in this study to be applicable with confidence to scenarios similar to that presented here.

Acknowledgements

This research was funded by a University of Glasgow Postgraduate Scholarship and a British Geological Survey University Funding Initiative (BUFI) Scholarship. Funding from the Scottish Alliance for Geoscience, Environment and Society (SAGES) is also acknowledged. We thank Maarten Lupker and an anonymous reviewer for helpful comments and suggestions.

References

Alford, D., 1992. Streamflow and sediment transport from mountain watersheds of the Chao Phraya basin, Northern Thailand: a reconnaissance study. Mountain Research and Development 12, 257–268.

Anderson, R.S., Humphrey, N.F., 1989. Interaction of weathering and transport processes in the evolution of arid landscapes, in: Cross, T.A. (Ed.), Quantitative Dynamic Stratigraphy. Prentice-Hall, Englewood Cliffs, pp. 349–361.

Anderson, R.S., Repka, J., Dick, G., 1996. Explicit treatment of inheritance in dating depositional surfaces using in situ ^{10}Be and ^{26}Al. Geology 24, 47–51.

Anselmetti, F.S., Hodell, D.A., Ariztegui, D., Brenner, M., Rosenmeier, M.F., 2007. Quantification of soil erosion rates related to ancient Maya deforestation. Geology 35, 915–918.

Ascough, P.L., Cook, G.T., Dugmore, A.J., 2009. North Atlantic marine ^{14}C reservoir effects: Implications for late-Holocene chronological studies. Quaternary Geochronology 4, 171–180.

Balco, G., Stone, J.O., 2003. Measuring the density of rock, sand, till, etc. http://depts.washington.edu/cosmolab/chem.html 26. August 2011.

Balco, G., Stone, J.O., Lifton, N.A., Dunai, T.J., 2008. A complete and easily accessible means of calculating surface exposure ages or erosion rates from ^{10}Be and ^{26}Al measurements. Quaternary Geochronology 3, 174–195.

Ballantyne, C.K., 1984. The Late Devensian periglaciation of upland Scotland. Quaternary Science Reviews 3, 311–343.

Barg, E., Lal, D., Pavich, M.J., Caffee, M.W., Southon, J.R., 1997. Beryllium geochemistry in soils: evaluation of ^{10}Be/ ^{9}Be ratios in authigenic minerals as a basis for age models. Chemical Geology 140, 237–258.

Barrett, J.C., 1981. Aspects of the Iron Age in Atlantic Scotland. A case study in the problems of achaelogical interpretation. Proceedings of the Society of Antiquaries of Scotland 111.

Benn, D.I., 1992. The genesis and significance of 'hummocky moraine': evidence from the Isle of Skye, Scotland. Quaternary Science Reviews 11, 781–799.

Benn, D.I., Lukas, S., 2006. Younger Dryas glacial landsystems in North West Scotland: an assessment of modern analogues and palaeoclimatic implications. Quaternary Science Reviews 25, 2390–2408.

Bevington, P.R., Robinson, K.D., 2003. Data Reduction and Error Analysis for the Physical Sciences. McGraw-Hill, Boston MA.

Bierman, P.R., 2007. Cosmogenic glacial dating, 20 years and counting. Geology 35, 575–576.

Bierman, P.R., Nichols, K.K., 2004. Rock to sediment - slope to sea with ^{10}Be - rates of landscape change. Annual Review of Earth and Planetary Sciences 32, 215–255. doi:10.1146/annurev.earth.32.101802.120539.

Bishop, P., 2007. Long-term landscape evolution: linking tectonics and surface processes. Earth Surface Processes and Landforms 32, 329–365. doi:10.1002/esp.1493.

Borren, W., Bleuten, W., Lapshina, E.D., 2004. Holocene peat and carbon accumulation rates in the southern taiga of western Siberia. Quaternary Research 61, 42–51.

Bradwell, T., Fabel, D., Stoker, M.S., Mathers, H., McHargue, L.R., Howe, J.A., 2008. Ice caps existed throughout the Lateglacial Interstadial in northern Scotland. Journal of Quaternary Science 23, 401–407.

Braucher, R., Brown, E.T., Bourlès, D.L., Colin, F., 2003. In situ produced ^{10}Be measurements at great depths: implications for production rates by fast muon. Earth and Planetary Science Letters 211, 251–258.

Braucher, R., Colin, F., Brown, E.T., Bourlès, D.L., Bamba, O., Raisbeck, G.M., Yiou, F., Koud, J.M., 1998. African laterite dynamics using in situ-produced ^{10}Be. Geochimica and Cosmochimica Acta 62, 1501–1507.

Braucher, R., Del Castillo, P., Siame, L., Hidy, A.J., Bourlès, D.L., 2009. Determination of both exposure time and denudation rate from an in situ-produced ^{10}Be depth profile: A mathematical proof of uniqueness. Model sensitivity and applications to natural cases. Quaternary Geochronology 4, 56–67.

Briner, J.P., Swanson, T.W., 1998. Using inherited cosmogenic ^{36}Cl to constrain glacial erosion rates of the Cordilleran ice sheet. Geology 26, 3–6.

Bronk Ramsey, C., Lee, S., 2013. Recent and planned developments of the program OxCal. Radiocarbon 55, 720–730.

Brown, E.T., Bourlès, D.L., Colin, F., Sanfo, Z., Raisbeck, G.M., Yiou, F., 1994. The development of iron crust lateritic systems in Burkina Faso, West Africa examined with in-situ-produced cosmogenic nuclides. Earth and Planetary Science Letters 124, 19–33.

Brown, E.T., Stallard, R.F., Larsen, M.C., Raisbeck, G.M., Yiou, F., 1995. Denudation rates determined from the accumulation of in situ-produced ^{10}Be in the Luquillo Experimental Forest, Puerto Rico. Earth and Planetary Science Letters 129, 193–202.

Brown, R.M., Andrews, H.R., Ball, G.C., Burn, N., Imahori, Y., Milton, J.C.D., Fireman, E.L., 1984. ^{14}C content of ten meteorites measured by tandem accelerator mass spectrometry. Earth and Planerary Science Letters 67, 1–8.

Browne, M.A.E., Graham, D.K., 1981. Glaciomarine deposits of the Loch Lomond Stade glacier in the Vale of Leven between Dumbarton and Balloch, west-central Scotland. Quaternary Newsletter 34, 1–7.

Buechi, M.W., Kober, F., Ivy-Ochs, S., Salcher, B., Kubik, P.W., Christl, M., 2014. Denudation rates of small transient catchements controlled by former glaciation: the Hörnli nunatak in the northeastern Swiss Alpine Foreland. Quaternary Geochronology 19, 135–147.

Child, D., Elliott, G., Mifsud, C., Smith, A.M., Fink, D., 2000. Sample processing for earth science studies at ANTARES. Nuclear Instruments and Methods in Physics Research B 172, 856–860.

Chmeleff, J., von Blanckenburg, F., Kossert, K., Jakob, D., 2010. Determination of the ^{10}Be half-life by multicollector ICP-MS and liquid scintillation counting. Nuclear Instruments & Methods In Physics Research Section B-Beam Interactions With Materials and Atoms 268, 192–199.

Clapp, E.M., Bierman, P.R., Schick, A.P., Lekach, J., Enzel, Y., Caffee, M.W., 2000. Sediment yield exceeds sediment production in arid region drainage basins. Geology 28, 995–998.

Cook, G.T., Dugmore, A.J., Shore, J.S., 1998. The influence of pretreatment on humic acid yield and ^{14}C age of carex peat. Radiocarbon 40, 21–27.

Coope, G.R., Rose, J., 2008. Palaeotemperatures and palaeoenvironments during the Younger Dryas: Arthropod evidence from Croftamie at the type area of the Loch Lomond Readvance, and significance for the timing of glacier expansion during the Lateglacial period in Scotland. Scottish Journal of Geology 44, 43–49.

Cornu, S., Montagne, D., Vasconcelos, P.M., 2009. Dating constituent formation in soils to determine rates of soil processes: A review. Geoderma 153, 293–303.

Daniels, B., Gilliam, J.W., Cassel, D.K., Nelson, L.A., 1987. Quantifying the effects of past soil erosion on present soil productivity. Journal of Soil and Water Conservation 42, 183–187.

Douglass, D., Bockheim, J., 2006. Soil-forming rates and processes on Quaternary moraines near Lago Buenos Aires, Argentina. Quaternary Research 65, 293–307.

Duck, R.W., McManus, J., 1987. Soil erosion near Barry, Angus. Scottish Geographical Magazine 103, 44–46.

Dugan, B., 2008. New Production Rate Estimates for In Situ Cosmogenic ^{14}C from Lake Bonneville, Utah, and Northwestern Scotland. Master's thesis. University of Arizona. Tucson.

Dunai, T.J., 2010. Cosmogenic Nuclides: Principles, Concepts and Applications in the Earth Surface Sciences. Cambridge Univeristy Press.

Dunne, J., Elmore, D., Muzikar, P., 1999. Scaling factors for the rates of production of cosmogenic nuclides for geometric shielding and attenuation at depth on sloped surfaces. Geomorphology 27, 3–11.

Edwards, K.J., Whittington, G., 2001. Lake sediments, erosion and landscape change during the Holocene in Britain and Ireland. Catena 42, 143–173.

Evans, D.J.A., Rose, J., 2003. Late Quaternary stratigraphy of the Western Highland Boundary, in: Evans, D.J.A. (Ed.), The Quaternary of the Western Highland Boundary - Field Guide. Quaternary Research Association, pp. 21–29.

Evans, D.J.A., Wilson, S.B., 2006. Scottish landform example 39: The Lake of Menteith glacitectonic hill-hole pair. Scottish Geographical Journal 122, 352–364.

Evans, D.J.A., Wilson, S.B., Rose, J., 2003. Glacial geomorphology of the western highland boundary, in: Evans, D.J.A. (Ed.), The Quaternary of the Western Highland Boundary - Field Guide. Quaternary Research Association, pp. 5–20.

Fabel, D., Stroeven, A.P., Harbor, J., Kleman, J., Elmore, D., Fink, D., 2002. Landscape preservation under fennoscandian ice sheets determined from in situ produced ^{10}Be and ^{26}Al. Earth and Planerary Science Letters 201, 397–406.

Fausey, N.R., Hall, G.F., Bigham, J.M., Allred, B.J., Christy, A.D., 2000. Properties of the fractured glacial till at the Madison County, Ohio, Field Workshop Pit Site. The Ohio Journal of Science 100, 107–112.

Freeman, S.P.H.T., Bishop, P., Bryant, C., Cook, G., Dougans, D., Ertunc, T., Fallick, A., Ganeshram, R., Maden, C., Naysmith, P., Schnabel, C., Scott, M., Summerfield, M.A., Xu, S., 2007. The SUERC AMS laboratory after 3 years. Nuclear Instruments and Methods in Physics Research B 259, 66–70.

Fuchs, M., 2007. An assessment of human versus climatic impacts on Holocene soil erosion in NE Peloponnese, Greece. Quaternary Research 67, 349–356.

Fuchs, M., Lang, A., 2001. OSL dating of coarse-grain fluvial quartz using single-aliquot protocols on sediments from NE Peloponnese, Greece. Quaternary Science Reviews 20, 783–787.

Fülöp, R.H., Naysmith, P., Cook, G.T., Fabel, D., Xu, S., Bishop, P., 2010. Update on the performance of the SUERC in situ cosmogenic ^{14}C extraction line. Radiocarbon 52, 1288–1294.

Gale, S.J., Hoare, P.G., 1991. Quaternary Sediments. John Wiley & Sons, New York.

Gerrard, J., 1992. Soil Geomorphology, an integration of pedology and geomorphology. Chapman and Hall, London.

Golledge, N.R., 2010. Glaciation of Scotland during the Younger Dryas stadial: a review. Journal of Quaternary Science 25, 550–566.

Golledge, N.R., Fabel, D., Everest, J.D., Freeman, S., S., B., 2007. First cosmogenic ^{10}Be age constraint on the timing of Younger Dryas glaciation and ice cap thickness, western Scottish Highlands. Journal of Quaternary Science 22, 785–791.

Golledge, N.R., Hubbard, A., 2005. Evaluating Younger Dryas glacier reconstructions in part of the western Scottish Highlands: a combined empirical and theoretical approach. Boreas 34, 274–286.

Golledge, N.R., Hubbard, A., Sugden, D.E., 2008. High-resolution numerical simulation of Younger Dryas glaciation in Scotland. Quaternary Science Reviews 27, 888–904.

Gordon, J.E., 1982. Croftamie, in: Gordon, J.E., Sutherland, D.G. (Eds.), Geological Conservation Review Series. Chapman and Hall, London. volume 6: Quaternary of Scotland. chapter 13: Western Highland Boundary, p. 695.

Granger, D.E., Muzikar, P.F., 2001. Dating sediment burial with in situ-produced cosmogenic nuclides: theory, techniques, and limitations. Earth and Planetary Science Letters 188, 269–281.

Granger, D.E., Smith, A.L., 2000. Dating buried sediments using radioactive decay and muogenic production of ^{26}Al and ^{10}Be. Instruments and Methods in Physics Research B 172, 822–826.

Gulliksen, S., Scott, E.M., 1995. Report of the TIRI workshop, Saturday, 13 August 1994. Radiocarbon 37, 820–821.

Guralnik, B., Matmon, A., Avni, Y., Porat, N., Fink, D., 2010. Constraining the evolution of river terraces with integrated OSL and cosmogenic nuclide data. Quaternary Geochronology 6, 22–32.

Hallet, B., Putkonen, J.K., 1994. Surface dating of dynamic landforms: Young boulders on aging moraines. Science 265, 937–940.

Harden, J.W., Sundquist, E.T., Stallard, R.F., Mark, R.K., 1992. Dynamics of soil carbon during deglaciation of the Laurentide Ice Sheet. Science 258, 1921–1924.

Heimsath, A.M., Chappell, J., Dietrich, W.E., Nishiizumi, K., Finkel, R.C., 2000. Soil production on a retreating escarpment in southeastern Australia. Geology 28, 787–790.

Heimsath, A.M., Dietrich, W.E., Nishiizumi, K., Finkel, R.C., 1997. The soil production function and landscape equilibrium. Nature 388, 358–361.

Heimsath, A.M., Dietrich, W.E., Nishiizumi, K., Finkel, R.C., 1999. Cosmogenic nuclides, topography, and the spatial variation of soil depth. Geomorphology 27, 151–172.

Hein, A.S., Hulton, N.R.J., Dunai, T.J., Schnabel, C., Kaplan, M.R., Naylor, M., Xu, S., 2009. Middle Pleistocene glaciation in Patagonia dated by cosmogenic-nuclide measurements on outwash gravels. Earth and Planetary Science Letters 286, 184–197.

Heisinger, B., Lal, D., Jull, A.J.T., Kubik, P., Ivy-Ochs, S., Knie, K., Nolte, E., 2002b. Production of selected cosmogenic radionuclides by muons. 2: Capture of negative muons. Earth and Planerary Science Letters 200, 357–369.

Heisinger, B., Lal, D., Jull, A.J.T., Kubik, P., Ivy-Ochs, S., Neumaier, S., Knie, K., Lazarev, V., Nolte, E., 2002a. Production of selected cosmogenic radionuclides by muons. 1: Fast muons. Earth and Planetary Science Letters 200, 345–355.

Heisinger, B., Niedermayer, M., Hartmann, F.J., Korschinek, G., Nolte, E., Morteani, G., Neumaier, S., Petitjean, C., Kubik, P., Synal, A., Ivy-Ochs, S., 1997. In-situ production of radionuclides at great depths. Nuclear Instruments and Methods in Physics Research B 123, 341–346.

Herman, F., Seward, D., Valla, P.G., Carter, A., Kohn, B., Willett, S.D., Ehlers, T.A., 2013. Worldwide acceleration of mountain erosion under a cooling climate. Nature 504, 423–426.

Hewawasam, T., von Blanckenburg, F., Schaller, M., Kubik, P., 2003. Increase of human over natural erosion rates in tropical highlands constrained by cosmogenic nuclides. Geology 31, 597–600.

Heyman, J., 2014. Paleoglaciation of the Tibetan Plateau and surrounding mountains based on exposure ages and ELA depression estimates. Quaternary Science Reviews 91, 30–41.

Hidy, A.J., Gosse, J., Pederson, J.L., Mattern, J.P., Finkel, R.C., 2010. A geologically constrained Monte Carlo approach to modeling exposure ages from profiles of cosmogenic nuclides: An example from Lees Ferry, Arizona. Geochemistry Geophysics Geosystems 11, 1–18.

Hippe, K., Kober, F., Wacker, L., Fahrni, S.M., Ivy-Ochs, S., Akçar, N., Schlüchter, C., Wieler, R., 2013. An update on in situ cosmogenic 14C analysis at ETH Zürich. Nuclear Instruments & Methods In Physics Research Section B-Beam Interactions With Materials and Atoms 294, 81–86.

Hippe, K., Kober, F., Zeilinger, G., Ivy-Ochs, S., Maden, C., Wacker, L., Kubik, P.W., Wieler, R., 2012. Quantifying denudation rates and sediment storage on the eastern Altiplano, Bolivia, using cosmogenic Be-10, Al-26, and in situ C-14. Geomorphology 179, 58–70.

Hofmann, H.J., Beer, J., Bonani, G., Gunten, H.R.V., Raman, S., Suter, M., Walker, R.L., Wölfli, W., Zimmermann, D., 1987. ^{10}Be: Half-life and AMS-standards. Nuclear Instruments and Methods In Physics Research B 29, 32–36.

Hooke, R.L., 2000. On the history of humans as geomorphic agents. Geology 28, 843–846.

Howe, J.A., Shimmield, T., Austin, W.E.N., Longva, O., 2002. Post-glacial depositional environments in a mid-high latitude glacially-overdeepened sea loch, inner Loch Etive, western Scotland. Marine Geology 185, 417–433.

Inn, K.G.W., Raman, S., Coursey, B.M., Fassett, J.D., Walker, R.L., 1987. Development of the NBS ^{10}Be/^{9}Be isotopic standard reference material. Nuclear Instruments and Methods In Physics Research B 29, 27–31.

Jack, L., 1877. Notes on a till or boulder clay with broken shells, in the lower valley of the river Endrik, near Loch Lomond, and its relation to certain other glacial deposits. Transactions of the Geological Society of Glasgow V, 1–25.

Jull, A.J.T., Scott, E.M., Bierman, P., 2013. The CRONUS-Earth intercomparison for cosmogenic isotope analysis. Quaternary Geochronology , 1–8.

Kim, K.J., Englert, P.A.J., 2004. Profiles of in situ ^{10}Be and ^{26}Al at great depths at the Macraes Flat, East Otago, New Zealand. Earth and Planerary Science Letters 223, 113–126.

Kirkbride, M.P., Reeves, A.D., 1993. Soil erosion caused by low-intensity rainfall in Angus, Scotland. Applied Geography 13, 299–311.

Kohl, C.P., Nishiizumi, K., 1992. Chemical isolation of quartz for measurement of in-situ-produced cosmogenic nuclides. Geochimica et Cosmochimica Acta 56, 3583–3587.

Korschinek, G., Bergmaier, A., Faestermann, T., Gerstmann, U.C., Knie, K., Rugel, G., Wallner, A., Dillmann, I., Dollinger, G., Lierse von Gostomski, C., Kossert, K., Maiti, M., Poutivtsev, M., Remmert, A., 2010. A new value for the half-life of ^{10}Be by Heavy-Ion Elastic Recoil Detection and liquid scintillation counting. Nuclear Instruments & Methods In Physics Research Section B-Beam Interactions With Materials and Atoms 268, 187–191.

Kubik, P.W., Christl, M., Alfimov, V., 2009. New Primary Be-10 Standard and T1/2 for AMS at ETH. Technical Report. Ion Beam Physics, ETH Zürich.

Lal, D., 1991. Cosmic ray labeling of erosion surfaces - In situ nuclide production rates and erosion models. Earth and Planetary Science Letters 104, 424–439.

Lal, R., 2004. Soil carbon sequestration impacts on global climate change and food security. Science 304, 1623–1627.

Lal, R., 2005. Soil erosion and carbon dynamics. Soil & Tillage Research 81, 137–142.

Lifton, N., Sato, T., Dunai, T.J., 2014. Earth and Planetary Science Letters. Earth and Planetary Science Letters 386, 149–160.

Lifton, N.A., Bieber, J.W., Clem, J.M., Duldig, M.L., Evenson, P., Humble, J.E., Pyle, R., 2005. Addressing solar modulation and long-term uncertainties in scaling secondary cosmic rays for in situ cosmogenic nuclide applications. Earth and Planerary Science Letters 239, 140–161.

Lifton, N.A., Jull, A.J.T., Quade, J., 2001. A new extraction technique and production rate estimate for in situ cosmogenic ^{14}C in quartz. Geochimica et Cosmochimica Acta 65, 1953–1969.

Lifton, N.A., Smart, D.F., Shea, M.A., 2008. Scaling time-integrated in situ cosmogenic nuclide production rates using a continuous geomagnetic model. Earth and Planerary Science Letters 268, 190–201.

Lowell, T.V., 2000. As climate changes, so do glaciers. Proceedings of the National Academy of Sciences of the United States of America 97, 1351–1354.

Lowell, T.V., Savage, K.M., Brockman, S.C., Stuckenrath, R., 1990. Radiocarbon analyses from Cincinnati, Ohio, and their implications for glacial stratigraphic interpretations. Quaternary Research 34, 1–11.

Ma, L., Chabaux, F., Pelt, E., Blaes, E., Jin, L., Brantley, S., 2010. Regolith production rates calculated with uranium-series isotopes at Susquehanna/Shale Hills Critical Zone Oobservatory. Earth and Planetary Science Letters 297, 211–225.

Maden, C., Anastasi, P., Dougans, D., Freeman, S., Kitchen, R., Klody, G., 2007. SUERC AMS ion detection. Nuclear Instruments and Methods in Physics Research B 259, 131–139.

McIntyre, K.L., Howe, J.A., 2010. Scottish west coast fjords since the last glaciation: a review. volume Special Publications 344. Geological Society, London.

McKean, J.A., Dietrich, W.E., Finkel, R.C., Southon, J.R., Caffee, M.W., 1993. Quantification of soil production and downslope creep rates from cosmogenic ^{10}Be accumulations on a hillslope profile. Geology 21, 343–346.

Middleton, R., Brown, L., Dezfouly-Arjomandy, B., Klein, J., 1993. On ^{10}Be standards and the half-life of ^{10}Be. Nuclear Instruments and Methods In Physics Research B 82, 399–403.

Milliman, J.D., Qin, Y.S., Ren, M.E., Saito, Y., 1987. Man's influence on the erosion and transport of sediment by Asian rivers: the Yellow River (Huanghe) example. Journal of Geology 95, 751–762.

Molnar, P., England, P., 1990. Late Cenozoic uplift of mountain ranges and global climate change: chicken or egg? Nature 346, 29–34.

Montgomery, D.R., 2007. Dirt: The Erosion of Civilizations. University of California Press.

Naysmith, P., Cook, G.T., Phillips, W., Lifton, N.A., Anderson, R., 2004. Preliminary results for the extraction and measurement of cosmogenic in situ ^{14}C from quartz. Radiocarbon 46, 201–206.

Niedermann, S., 2002. Cosmic-ray-produced noble gases in terrestrial rocks: Dating tools for surface processes, in: Porcelli, D.P., Ballentine, C.J., Wieler, R. (Eds.), Noble Gases. The Mineralogical Society of America. volume 47 of *Reviews in Mineralogy and Geochemistry*, pp. 731–784.

Heier Nielsen, S., Heinemeier, J., Nielsen, H.L., Rud, N., 1995. Recent reservoir ages for Danish fjords and marine waters. Radiocarbon 37, 875–882.

Nishiizumi, K., Imamura, M., Caffee, M.V., Southon, J.R., Finkel, R.C., Mcaninch, J., 2007. Absolute calibration of ^{10}Be ams standards. Nuclear Instruments & Methods In Physics Research Section B-Beam Interactions With Materials and Atoms 258, 403–413.

O'Neal, M.A., 2006. The effects of slope degradation on lichenometric dating of Little Ice Age moraines. Quaternary Geochronology 1, 121–128.

Palmer, A.P., Rose, J., Lowe, J., Macleod, A., 2010. Annually resolved events of Younger Dryas glaciation in Lochaber (Glen Roy and Glen Spean), Western Scottish Highlands. Journal of Quaternary Science 25, 581–596.

Pelletier, J.D., 2008. Quantitative modeling of earth surface processes. Cambridge University Press.

Perg, L.A., Anderson, R.S., Finkel, R.C., 2001. Use of a new ^{10}Be and ^{26}Al inventory method to date marine terraces, Santa Cruz, California, USA. Geology 29, 879–882.

Phillips, E.R., Evans, D.J.A., Auton, C.A., 2002. Polyphase deformation at an oscillating ice margin following the Loch Lomond Readvance, central Scotland, UK. Sedimentary Geology 149, 157–182.

Phillips, W.M., McDonald, S.L., Reneau, S.L., Poths, J., 1998. Dating soils and alluvium with cosmogenic ^{21}Ne depth profiles: case studies from the Pajarito Plateau, New Mexico, USA. Earth and Planetary Science Letters 160, 209–223.

Pigati, J.S., Lifton, N.A., Jull, A.J.T., Quade, J., 2010. A simplified in situ cosmogenic ^{14}C extraction system. Radiocarbon 52, 1236–1243.

Pimentel, D., Harvey, C., Resosudarmo, P., Sinclair, K., Kurz, D., Mcnair, M., Crist, S., Shpritz, L., Fitton, L., Saffouri, R., Blair, R., 1995. Environmental and economic costs of soil erosion and conservation benefits. Science 267, 1117–1123.

Putkonen, J.K., Connolly, J., Orloff, T., 2007. Landscape evolution degrades the geologic signature of past glaciations. Geomorphology 97, 208–217.

R Core Team, 2014. R: A Language and Environment for Statistical Computing. R Foundation for Statistical Computing. Vienna, Austria. URL: `http://www.R-project.org/`.

Reimer, P., Bard, E., Bayliss, A., Beck, J., Blackwell, P., Bronk Ramsey, C., Buck, C., Cheng, H., Edwards, R.L., Friedrich, M., Grootes, P., Guilderson, T., Haflidason, H., Hajdas, I., Hatt, C., Heaton, T., Hoffmann, D., Hogg, A., Hughen, K., Kaiser, K., Kromer, B., Manning, S., Niu, M., Reimer, R., Richards, D., Scott, E., Southon, J., Staff, R., Turney, C., van der Plicht, J., 2013. IntCal13 and Marine13 radiocarbon age calibration curves 050,000 years cal BP. Radiocarbon 55, 1869–1887.

Riebe, C.S., Kirchner, J.W., Finkel, R.C., 2003. Long-term rates of chemical weathering and physical erosion from cosmogenic nuclides and geochemical mass balance. Geochimica et Cosmochimica Acta 67, 4411–4427.

Rodés, A., Pallás, R., Braucher, R., Moreno, X., Masana, E., Bourlès, D.L., 2011. Effect of density uncertainties in cosmogenic ^{10}Be depth-profiles: Dating a cemented Pleistocene alluvial fan (Carboneras Fault, SE Iberia). Quaternary Geochronology 6, 186–194.

Rose, J., Lowe, J.J., Switsur, R., 1989. A radiocarbon date on plant detritus beneath till from the type area of the Loch Lomond Readvance,. Scottish Journal of Geology 24, 113–124.

Schaller, M., von Blanckenburg, F., Hovius, N., Veldkamp, A., van de Berg, M.W., Kubik, P.W., 2004. Paleoerosion rates from cosmogenic ^{10}Be in a 1.3 Ma terrace sequence: Response of the River Muse to changes in climate and rock uplift. The Journal of Geology 112, 127–144.

Schaller, M., von Blanckenburg, F., Veit, H., Kubik, P.W., 2003. Influence of periglacial cover beds on in-situ produced cosmogenic ^{10}Be in soil sections. Geomorphology 49, 255–267.

Schaller, M., Blum, J.D., Ehlers, T.A., 2009. Combining cosmogenic nuclides and major elements from moraine soil profiles to improve weathering rate estimates. Geomorphology 106, 198–205.

Schaller, M., Ehlers, T.A., Blum, J.D., 2010. Soil transport on a moraine foreslope. Geomorphology 115, 117–128.

Schnabel, C., Reinhardt, L., Barrows, T.T., Bishop, P., Davidson, A., Fifield, L.K., Freeman, S., Kim, J.Y., Maden, C., Xu, S., 2007. Inter-comparison in ^{10}Be analysis starting from pre-purified quartz. Nuclear Instruments and Methods B 259, 571–575.

Schoenbohm, L., Kurz, M., Ackert, R., Brook, E., Brown, E.T., 2004. Erosion history from cosmogenic ^{3}He, ^{21}Ne, ^{10}Be and ^{26}Al depth profiles: Dry Valleys, Antarctica, in: Assembly, E.G. (Ed.), Geophysical Research Abstracts, p. EGU01062.

Scott, E.M., 2003. The Fourth International Radiocarbon Intercomparison (FIRI). Radiocarbon 45, 135–291.

Siame, L., Bellier, O., Braucher, R., Sebrier, M., Cushing, M., Bourlès, D.L., Hamelin, B., Baroux, E., de Voogd, B., Raisbeck, G., Yiou, F., 2004. Local erosion rates versus active tectonics: cosmic ray exposure modelling in Provence (South-East France). Earth and Planerary Science Letters 220, 345–364.

Sissons, J.B., 1967. Glacial stages and radiocarbon dates in Scotland, in: Scottish Journal of Geology III, Geological Societies of Edinburgh and Glasgow. Oliver & Boyd LTD. pp. 375–381.

Sissons, J.B., 1979. The Loch Lomond Stadial in the British Isles. Nature 280, 199–203.

Slota, P.J.J., Jull, A.J.T., Linick, T.W., Toolin, L.J., 1987. Preparation of small samples for ^{14}C accelerator targets by catalytic reduction of CO. Radiocarbon 29, 303–306.

Small, E.E., Anderson, R.S., Hancock, G.S., 1999. Estimates of the rates of regolith production using ^{10}Be and ^{26}Al from an alpine hillslope. Geomorphology 27, 131–150.

Smout, T.C., Fenton, A., 1965. Scottish Agriculture before the improvers-an Exploration. Agricultural History Review 13, 73–93.

Staiger, J.K.W., Gosse, J., Little, E.C., Utting, D.J., Finkel, R., Johnson, J.V., Fastook, J., 2006. Glacial erosion and sediment dispersion from detrital cosmogenic nuclide analyses of till. Quaternary Geochronology 1, 29–42.

Staiger, J.K.W., Gosse, J.C., Johnson, J.V., Fastook, J., Gray, J.T., Stockli, D.F., Stockli, L., Finkel, R.C., 2005. Quaternary relief generation by polythermal glacier ice. Earth Surface Processes and Landforms 30, 1145–1159.

Stone, C.O., Ballantyne, J.K., 2006. Dimensions and deglacial chronology of the Outer Hebrides Ice Cap, Northwest Scotland: implications of cosmic ray exposure dating. Journal of Quaternary Science 21, 75–84.

Stone, J.O., 2000. Air pressure and cosmogenic isotope production. Journal of Geophysical Research 105, 23753–23760.

Stone, J.O., Ballantyne, C.K., Fifield, L.K., 1998. Exposure dating and validation of periglacial weathering limits, northwest Scotland. Geology 26, 587–590.

Strack, E., Heisinger, B., Dockhorn, B., Hartmann, F.J., Korschinek, G., Nolte, E., Morteani, G., Petitjean, C., Neumaier, S., 1994. Determination of erosion rates with cosmogenic ^{26}Al. Nuclear Instruments and Methods in Physics Research Section B: Beam Interactions with Materials and Atoms 92, 317–320.

Stroeven, A.P., Fabel, D., Hattestrand, C., Harbor, J., 2002. A relict landscape in the centre of the Fennoscandian glaciation: cosmogenic radionuclide evidence of tors preserved through multiple glacial cycles. Geomorphology 44, 145–154.

Thorp, P.W., 1991. Surface profiles and basal shear stresses of outlet glaciers from a Late-glacial mountain ice field in western Scotland. Journal of Glaciology 37, 77–88.

Trimble, S.W., Crosson, P., 2000. Land use - US soil erosion rates - myth and reality. Science 289, 248–250.

Trumbore, S.E., 1993. Comparison of carbon dynamics in tropical and temperate soils using radiocarbon measurements. Global Biogeochemical Cycles 7, 275–290.

Tucker, G.E., Hancock, G.R., 2010. Modelling landscape evolution. Earth Surface Processes And Landforms 35, 28–50.

Walker, M.J.C., 1995. Climatic changes in Europe during the Last Glacial/Interglacial transition. Quaternary International 28, 63–76.

Walling, D., Webb, B., 1996. Erosion and sediment yield: a global overview, in: Erosion and Sediment Yield; Global and Regional Perspectives (Proceedings of the Exeter Symposium). IAHS. volume 236, pp. 3–19.

Wells, S.G., Mcfadden, L.D., Dohrenwend, J.C., 1987. Influence of Late Quaternary climatic changes on geomorphic and pedogenic processes on a desert piedmont, Eastern Mojave Desert, California. Quaternary Research 27, 130–146.

Wilkinson, B.H., McElroy, B.J., 2007. The impact of humans on continental erosion and sedimentation. Geological Society of America Bulletin 119, 140–156.

Wilkinson, M.T., Humphreys, G.S., 2005. Exploring pedogenesis via nuclide-based soil production rates and OSL-based bioturbation rates. Australian Journal of Soil Research 43, 767–779.

Willenbring, J.K., von Blanckenburg, F., 2010. Long-term stability of global erosion rates and weathering during late-Cenozoic cooling. Nature 465, 211–214.

Wilson, P., Bentley, M.J., Schnabel, C., Clark, R., Xu, S., 2008. Stone run (block stream) formation in the Falkland islands over several cold stages, deduced from cosmogenic isotope (^{10}Be and ^{26}Al) surface exposure dating. Journal of Quaternary Science 23, 461–473.

Xu, S., Anderson, R., Bryant, C., Cook, G.T., Dougans, A., Freeman, S.P.H.T., Naysmith, P., Schnabel, C., Scott, E.M., 2004. Capabilities of the new SUERC 5MV AMS Facility for ^{14}C dating. Radiocarbon 46, 51–58.

Xu, S., Dougans, A.B., Freeman, S.P.H.T., Schnabel, C., Wilcken, K.M., 2010. Improved 10Be and 26Al-AMS with a 5MV spectrometer. Nuclear Instruments & Methods In Physics Research Section B-Beam Interactions With Materials and Atoms 268, 736–738.

Yiou, F., Raisbeck, G.M., 1972. Half-life of ^{10}Be. Physical Review Letters 29, 372–375.

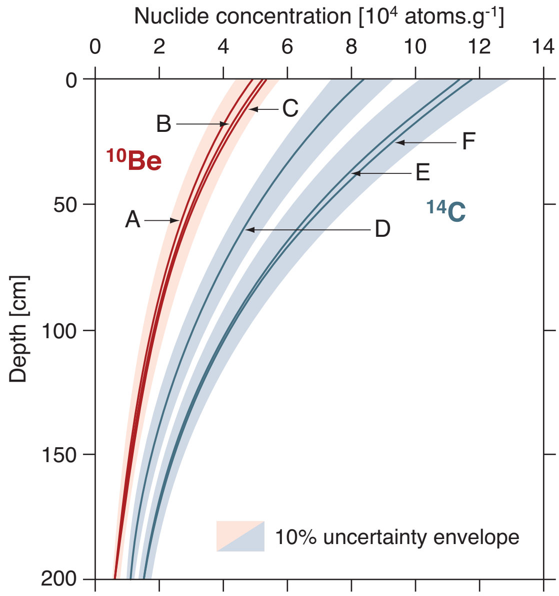

Figure 1: Hypothetical depth-profiles of concentrations of cosmogenic ^{10}Be and ^{14}C in a 10.5 kyr-old sedimentary deposit with various timings of surface erosion: A and D: 0 kyr (last few centuries); B and E: 4 kyr; and C and F: 6 kyr. Each depth-profile is the result of one erosion event removing 10 cm of material. In-situ ^{14}C discriminates better between the different scenarios because of its shorter half-life, enabling the distinguishing of Middle Holocene erosion events from modern. 10% uncertainty envelopes, covering production rate and analytical uncertainties, are conservative.

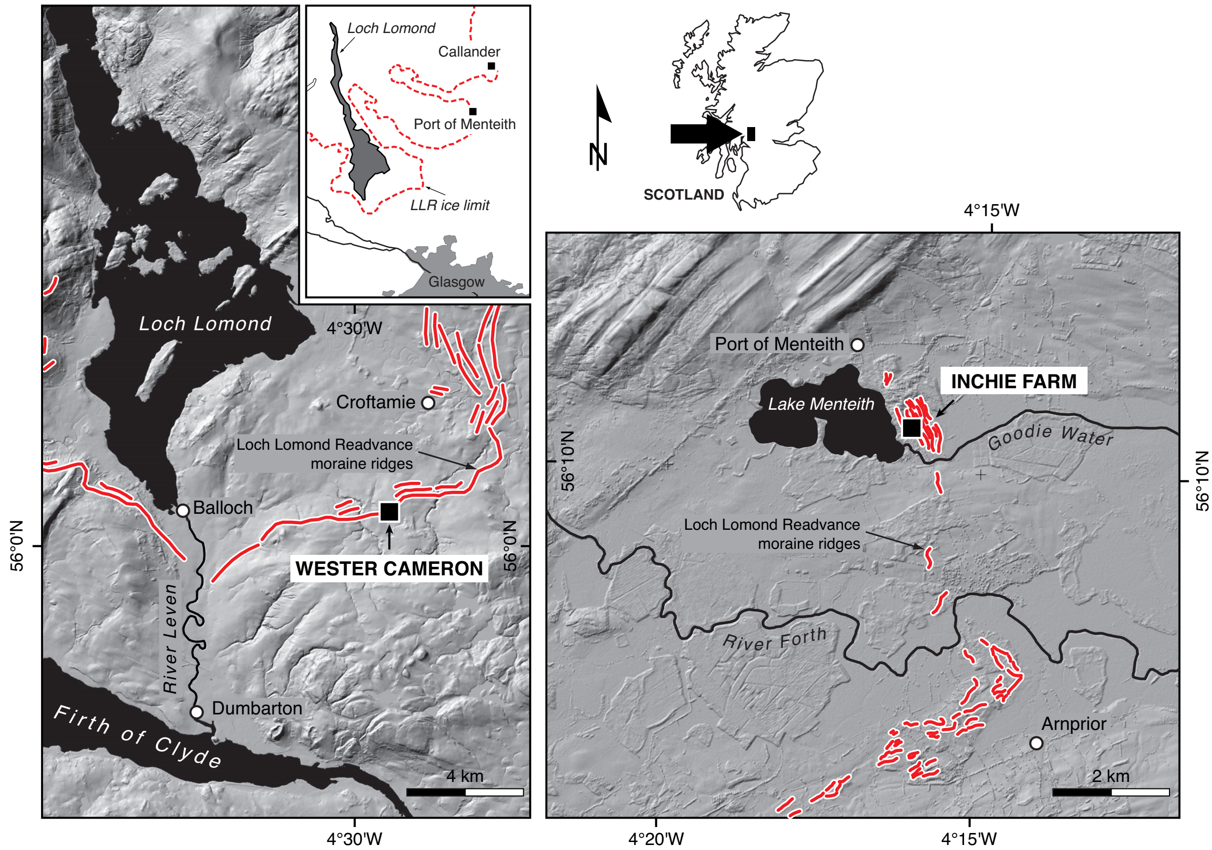

Figure 2: Map showing the location of the study sites. The locations of the Younger Dryas Loch Lomond Readvance (LLR) moraine ridges (in red) and LLR ice limit (inset) are based on data from Evans and Rose (2003); Evans et al. (2003), and Evans and Wilson (2006). DEM data courtesy of the British Geological Survey.

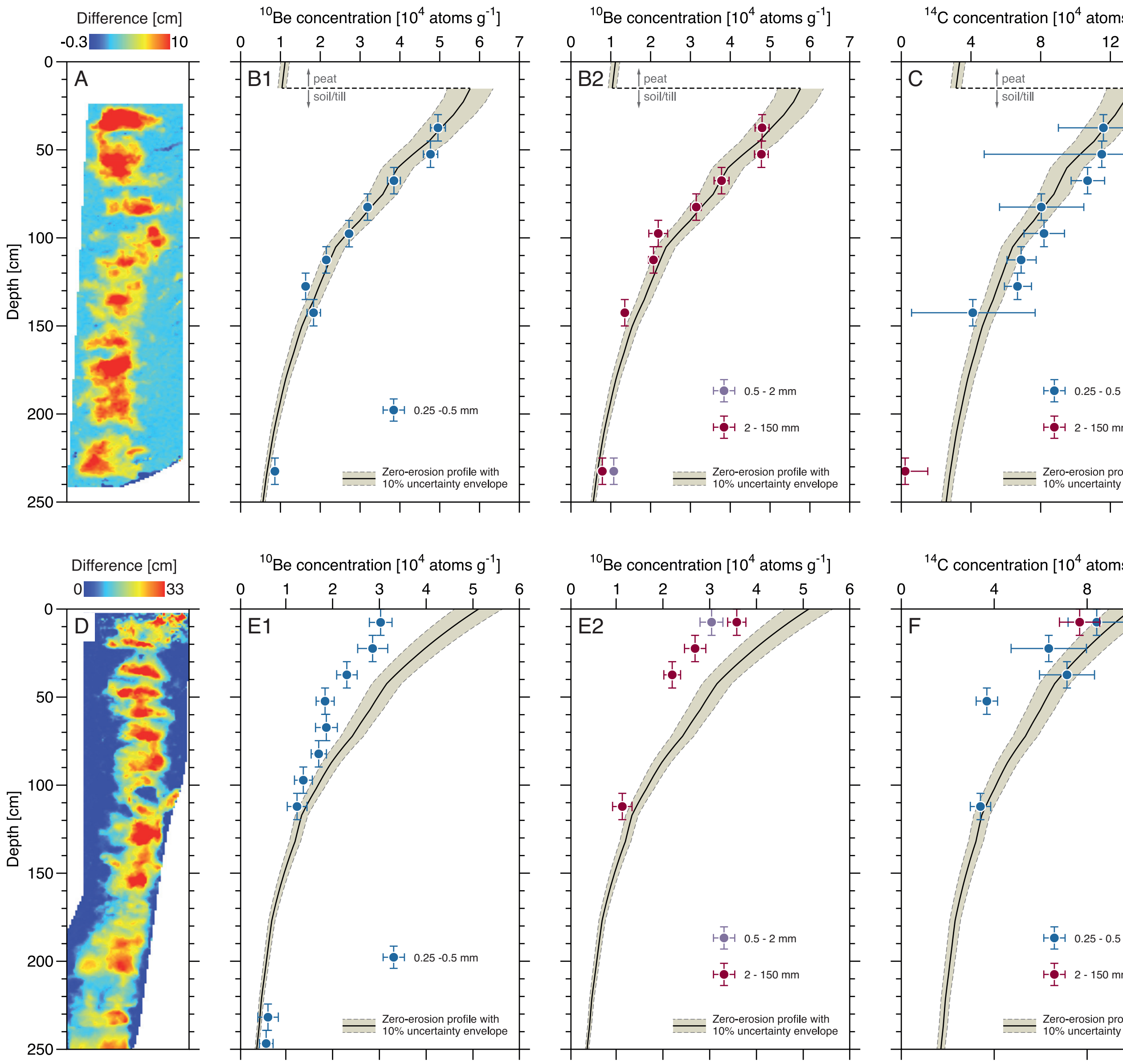

Figure 3: (A and D) Terrestrial laser scanner-derived plot of the thickness of material removed during sampling, and used for determining material density values. (B to F) Depth-profiles of measured ^{10}Be and ^{14}C concentrations at Wester Cameron (B and C) and Inchie Farm (E and F). Horizontal error bars represent measurement uncertainty at the 1σ level, and vertical error bars represent the sampling depth interval (15 cm). The *zero-erosion* depth profiles for the two sites were calculated assuming a till stabilisation age of 10.5 kyr (Table 1) and the bulk wet densities determined for the sampled profiles (A and D, and Table 3). In the case of the Wester Cameron pit, calculations also take into account capping by a peat layer with measured bulk density of ~0.8 g.cm^{-3}, developing at a constant rate from 2 kyr BP. See text for more details.

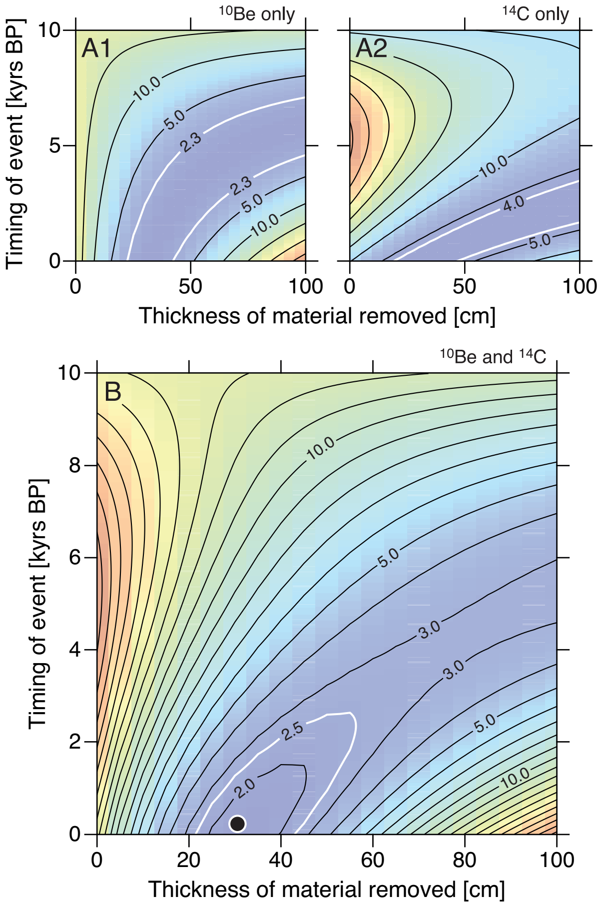

Figure 4: (A1 and A2) χ^2_{red} contour plots obtained for the ^{10}Be (A1) and ^{14}C (A2) depth-profiles used independently, and (B) χ^2_{red} contour plot obtained for the combined ^{10}Be and ^{14}C depth-profiles. Plots are obtained using an average wet density of $\rho = 1.82$ g.cm^{-3} and a zero continuous background erosion rate. White contours show the 68% (1σ) confidence envelope, and the black circle in (B) shows the erosional event timing and magnitude pair with the lowest χ^2_{red} (i.e., 1.5). Note how when the two nuclides are used independently (A), an infinite combination of erosional event magnitude and timing pairs produce fits with low χ^2_{red} values suggesting that ^{10}Be or ^{14}C on their own cannot constrain the magnitude and timing of a Holocene soil erosional event.

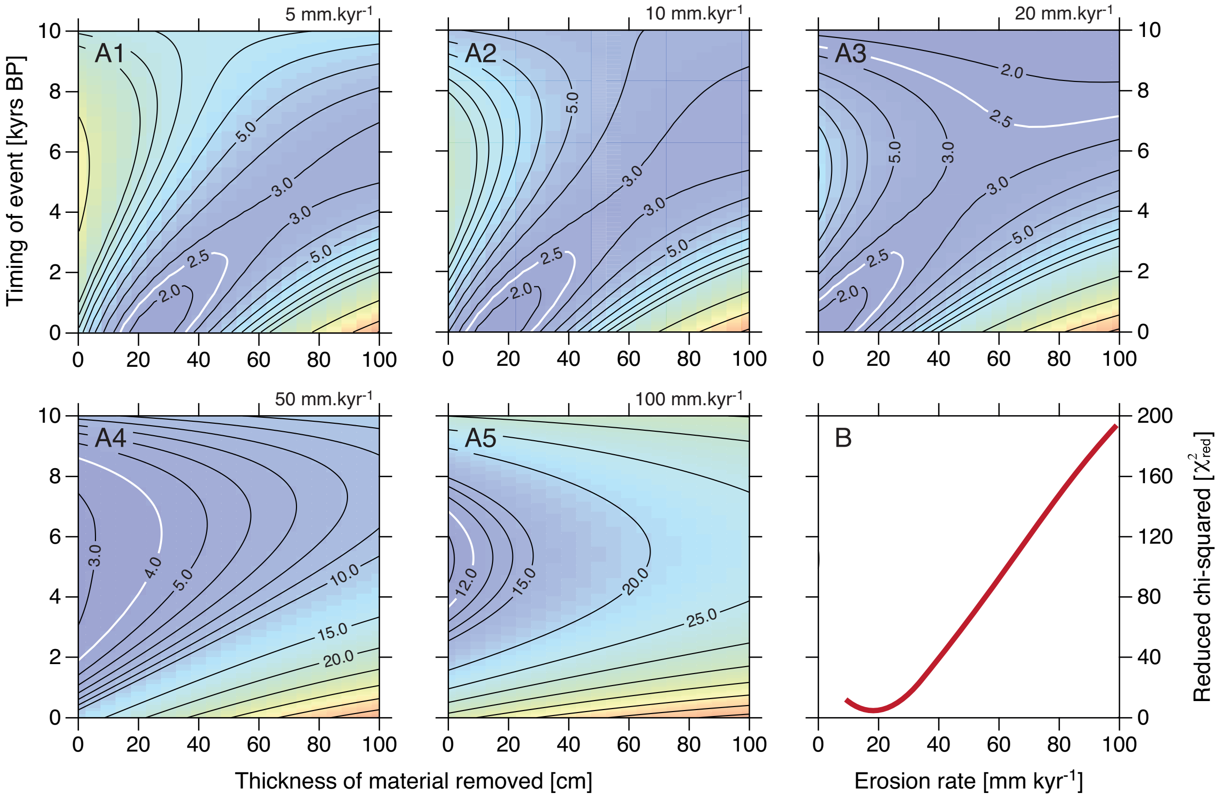

Figure 5: (A1 to A5) χ^2_{red} contour plots obtained for the combined ^{10}Be and ^{14}C depth-profiles for continuous background erosion rates of (A1) 5 mm.kyr^{-1}, (A2) 10 mm.kyr^{-1}, (A3) 20 mm.kyr^{-1}, (A4) 50 mm.kyr^{-1}, and (A5) 100 mm.kyr^{-1}. Plots are obtained using an average wet density of $\rho = 1.82$ g.cm^{-3}. White contours show the 68% (1σ) confidence envelope. (B) χ^2_{red} values obtained for the combined ^{10}Be and ^{14}C depth-profiles for continuous background erosion rates of 5 to 100 mm.kyr^{-1} and assuming no erosional events.

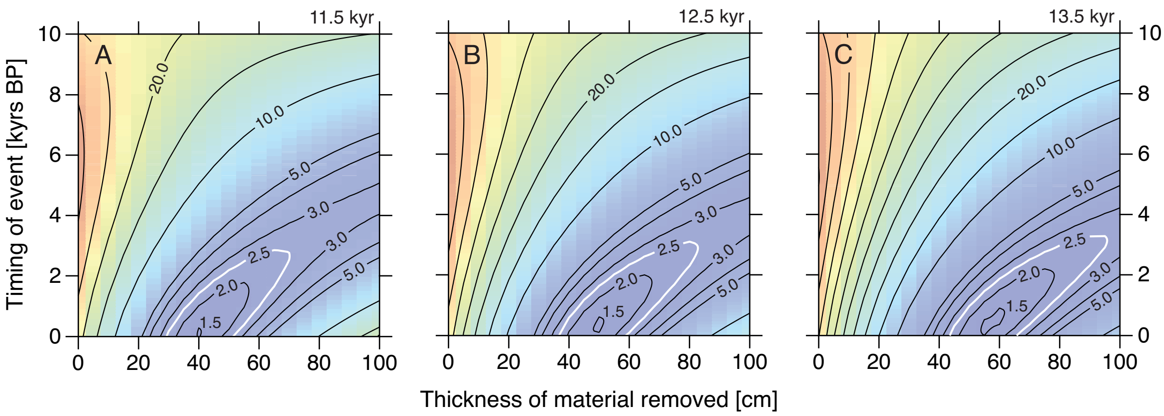

Figure 6: χ^2_{red} contour plots obtained for the combined ^{10}Be and ^{14}C depth-profiles assuming no continuous background erosion and a till stabilisation age of (A) 11.5 kyr, (B) 12.5 kyr, and (C) 13.5 kyr. Plots are obtained using an average wet density of $\rho = 1.82$ g.cm^{-3}. White contours show the 68% (1σ) confidence envelope.

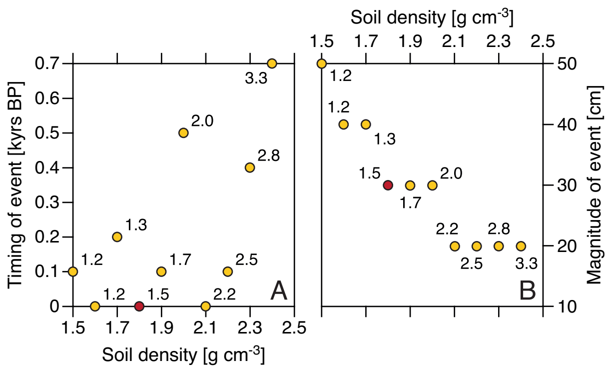

Figure 7: Predicted best-fit erosional event timing (A) and magnitude (B) as a function of assumed sedimentary deposit density. Values next to circles indicate minimum χ^2_{red} obtained for each density value varying at 0.1 g.cm^{-3} increments between 1.5 g.cm^{-3} and 2.4 g.cm^{-3}. Red circle represents best-fit erosional event timing and magnitude obtained for the mead density determined for the Inchie Farm site and used in this study.

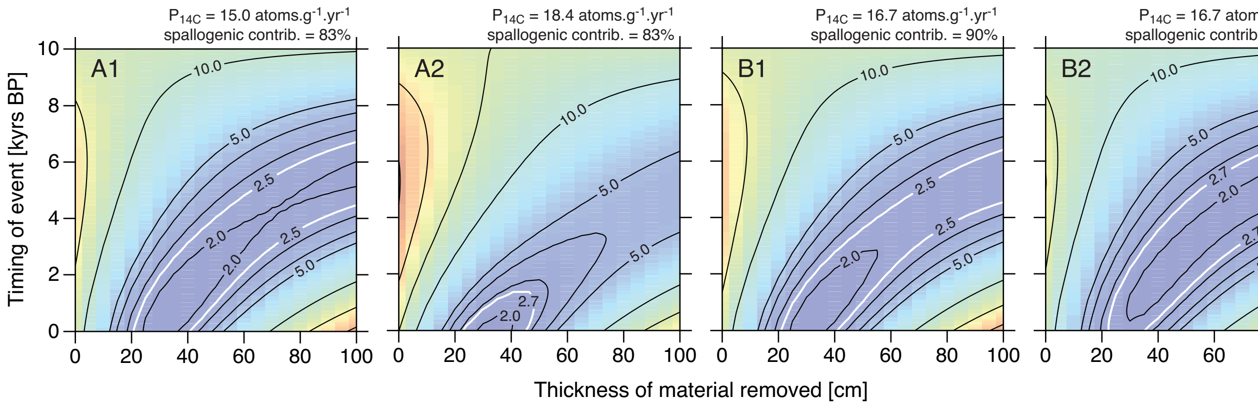

Figure 8: χ^2_{red} contour plots obtained for the combined ^{10}Be and ^{14}C depth-profiles assuming no continuous background erosion and: (A1) an in-situ ^{14}C SLHL production rate of 15.0 atoms.g^{-1}.yr^{-1}, 10% lower than the value calculated for the Inchie Farm site and used in this study, namely, 16.7 atoms.g^{-1}.yr^{-1}; (A2) an in-situ ^{14}C SLHL production rate of 18.4 atoms.g^{-1}.yr^{-1}, 10% higher than the value calculate for Inchie Farm; (B1) an in-situ ^{14}C SLHL production rate of 16.7 atoms.g^{-1}.yr^{-1} and assuming a spallogenic contribution of 90%, instead of the 83% reported in (Heisinger et al., 2002a,b); and (B2) same as in (B1) but assuming a spallogenic contribution of 100%. Plots are obtained using an average wet density of $\rho = 1.82$ g.cm^{-3}. White contours show the 68% (1σ) confidence envelope.

Table 1: Summary of in-situ ^{10}Be results in the Wester Cameron Farm erratic boulders.

Sample ID	Lat/Long[a] [degrees]	Elevation [m]	Thickness [cm]	^{10}Be production rate[b] [atoms.g^{-1}.yr^{-1}]		Shielding factor[c]	^{10}Be concentration[d,e,f] [$\times$ 10^3 atoms.g^{-1}]	Exposure age[b,f] [kyr]
				Neutrons	Muons			
Cameron A	56.0094 / -4.4741	155	2	5.28	0.191	0.9987	56.3 $\pm$ 1.8	10.6 $\pm$ 1.0
Cameron B	56.0094 / -4.4741	165	3	5.29	0.192	0.9985	55.2 $\pm$ 2.0	10.3 $\pm$ 1.0

[a] Latitude and longitude use WGS84 datum.

[b] Calculated with the CRONUS-Earth online calculator (v. 2.2, constants file v. 2.2.1; Balco et al., 2008), using the time dependent Lal/Stone scaling scheme.

[c] Calculated according to Dunne et al. (1999) based on field measurements.

[d] Corrected for a full chemistry procedural blank that yielded < 3% of the number of ^{10}Be atoms in the samples.

[e] Normalised to 2007 KNSTD (Nishiizumi et al., 2007) compatible with the updated ^{10}Be half-life of 1.387 $\pm$ 0.012 Myr (Chmeleff et al., 2010; Korschinek et al., 2010).

[f] All uncertainties reported at the 1σ level; uncertainties on exposure ages are external uncertainties.

Table 2: Results of the peat radiocarbon determinations.

SUERC ID	Depth [cm]	$\delta^{13}C$	Age $\pm$ 1σ [yrs]	Cal. age[a] [yrs BP]
19861	0.5 – 1.5	-29.8	1.166 $\pm$ 0.005	modern
19862	5.5 – 6.5	-28.8	800 $\pm$ 35	670 – 785
21602	6.0 – 8.0	-29.4	640 $\pm$ 35	550 – 670
21603	6.0 – 8.5	-31.0	625 $\pm$ 35	550 – 665
21596	6.5 – 8.5	-29.2	650 $\pm$ 35	550 – 675
19863	8.5 – 10.5	-28.9	610 $\pm$ 35	540 – 660
21601	9.0 – 10.0	-28.7	240 $\pm$ 35	20 – 430
21600	10.5 – 15.0	-29.1	125 $\pm$ 35	5 – 275

[a] Calibrated with Oxcal v.4.2 (Bronk Ramsey and Lee, 2013), using IntCal13 (Reimer et al., 2013).

Table 3: Summary of in-situ ^{10}Be results in the Wester Cameron and Inchie Farm depth-profiles.

Sample ID[a]	Depth [cm]	Dry density[b] [g.cm^{-3}]	Wet density[b] [g.cm^{-3}]	Quartz mass [g]	Be carrier mass[c] [μg]	^{10}Be/^{9}Be ratio[c,d] [$\times 10^{-15}$]	^{10}Be concentration[c,e,f] [$\times 10^{3}$ atoms.g^{-1}]
Wester Cameron Farm depth-profile[g]							
CPA-1F	30 – 45	0.92	1.34	33.00	197.8 ± 4.0	140.1 ± 4.4	49.50 ± 1.93
CPA-1P	30 – 45	0.92	1.34	33.01	197.7 ± 4.0	136.0 ± 3.9	48.00 ± 1.76
CPA-2F	45 – 60	1.65	1.99	33.03	198.2 ± 4.0	134.8 ± 4.0	47.68 ± 1.79
CPA-2P	45 – 60	1.65	1.99	33.01	197.6 ± 4.0	135.6 ± 3.8	47.82 ± 1.73
CPA-3F	60 – 75	0.95	1.10	35.04	164.4 ± 3.3	139.2 ± 4.9	38.50 ± 1.62
CPA-3P	60 – 75	0.95	1.10	15.01	163.9 ± 3.3	61.4 ± 2.3	37.82 ± 1.88
CPA-4F	75 – 90	1.71	1.96	35.03	164.2 ± 3.3	116.1 ± 4.0	31.87 ± 1.34
CPA-4P	75 – 90	1.71	1.96	25.15	163.5 ± 3.3	84.0 ± 2.8	31.46 ± 1.36
CPA-5F	90 – 105	2.16	2.52	35.02	164.0 ± 3.3	100.1 ± 3.6	27.28 ± 1.21
CPA-5P	90 – 105	2.16	2.52	7.03	134.6 ± 2.7	23.4 ± 1.7	21.92 ± 2.37
CPA-6F	105 – 120	1.21	1.41	34.43	163.5 ± 3.3	78.9 ± 2.9	21.51 ± 1.01
CPA-6P	105 – 120	1.21	1.41	19.91	163.7 ± 3.3	46.0 ± 2.6	20.73 ± 1.46
CPA-7F	120 – 135	1.31	1.55	34.89	163.5 ± 3.3	61.7 ± 2.4	16.32 ± 0.83
CPA-8F	135 – 150	1.74	2.03	34.57	163.4 ± 3.3	68.1 ± 5.4	18.31 ± 1.64
CPA-8P	135 – 150	1.74	2.03	34.55	163.8 ± 3.3	51.4 ± 2.3	13.52 ± 0.78
CPA-14F	225 – 240	1.67	1.96	26.89	163.3 ± 3.3	27.9 ± 1.6	8.61 ± 0.74
CPA-14M	225 – 240	1.67	1.96	13.12	133.0 ± 2.7	22.0 ± 1.5	10.75 ± 1.18
CPA-14P	225 – 240	1.67	1.96	30.75	163.1 ± 3.3	29.0 ± 1.9	7.89 ± 0.73
Inchie Farm depth-profile[h]							
LM-01F	0 – 15	1.35	1.85	21.98	236.1 ± 4.7	51.8 ± 3.0	30.28 ± 2.42
LM-01M	0 – 15	1.35	1.85	20.07	215.9 ± 4.3	51.9 ± 3.0	30.41 ± 2.42
LM-01P	0 – 15	1.35	1.85	24.46	215.7 ± 4.3	72.1 ± 2.7	35.79 ± 1.95
LM-02F	15 – 30	1.55	1.86	22.00	214.9 ± 4.3	53.5 ± 4.9	28.57 ± 3.21
LM-02P	15 – 30	1.55	1.86	19.97	218.1 ± 4.4	45.9 ± 2.7	26.91 ± 2.29
LM-03F	30 – 45	1.72	1.91	20.55	225.3 ± 4.5	40.0 ± 2.5	23.06 ± 2.19
LM-03P	30 – 45	1.72	1.91	20.32	211.4 ± 4.2	40.2 ± 1.9	21.99 ± 1.79
LM-04F	45 – 60	1.23	1.35	21.07	220.1 ± 4.4	34.4 ± 2.2	18.41 ± 1.93
LM-05F	60 – 75	1.41	1.60	22.06	222.2 ± 4.4	36.0 ± 3.2	18.68 ± 2.33
LM-06F	75 – 90	2.01	2.29	25.14	219.3 ± 4.4	37.6 ± 2.2	17.04 ± 1.62
LM-07F	90 – 105	1.81	2.05	20.59	220.4 ± 4.4	26.6 ± 2.1	13.76 ± 1.91
LM-08F	105 – 120	2.12	2.36	20.56	221.5 ± 4.4	24.5 ± 2.5	12.42 ± 2.11
LM-08P	105 – 120	2.12	2.36	21.52	190.4 ± 3.8	26.5 ± 3.3	11.32 ± 2.08
LM-16F	225 – 240	1.21	1.32	20.98	218.2 ± 4.4	15.4 ± 2.9	6.21 ± 2.19
LM-17F	240 – 255	1.77	1.96	20.15	220.0 ± 4.4	14.3 ± 1.0	5.82 ± 1.46

[a] Grains size fraction: F = 250 - 500 μm, M = 0.5 - 2 mm, P = 2 - 150 mm.

[b] Calculated using a terrestrial laser scanner. See text for full details.

[c] All uncertainties reported at the 1σ level.

[d] Isotope ratios were normalised to NIST SRM4325 using ^{10}Be/^{9}Be = 3.06×10^{-11} (Middleton et al., 1993) and a ^{10}Be half-life of 1.51 Myrs (Yiou and Raisbeck, 1972; Hofmann et al., 1987; Inn et al., 1987); Provided ^{10}Be/^{9}Be ratios are before blank correction.

[e] Normalised to 2007 KNSTD (Nishiizumi et al., 2007) compatible with the updated ^{10}Be half-life of 1.387 ± 0.012 Myr (Chmeleff et al., 2010; Korschinek et al., 2010).

[f] Corrected for full chemistry procedural blanks with ^{10}Be/^{9}Be ratios of $4.6 \pm 1.1 \times 10^{-15}$ (CPA samples) and $5.6 \pm 1.5 \times 10^{-15}$ (LM samples).

[g] Latitude: 56.00936 (WGS84); Longitude: -4.47410 (WGS84); Elevation: 169 m a.s.l.

[h] Latitude: 56.17488 (WGS84); Longitude: -4.27385 (WGS84); Elevation: 36 m a.s.l.

Table 4: Summary of in-situ ^{14}C results in the Wester Cameron and Inchie Farm depth-profiles.

Sample ID (AMS ID)[a]	Depth [cm]	Quartz mass[b] [g]	pMC[b]	δ^{13}C[b]	CO_2 [μg]	Blank[b] [$\times 10^5$ atoms]	Blank[c] [%]	^{14}C concentration[b] [$\times 10^3$ atoms.g^{-1}]
Wester Cameron Farm depth-profile[e]								
CPA-1F (g23001)	30 – 45	5.0014 ± 0.0005	2.785 ± 0.065	-0.8 ± 0.9	60.2	2.09 ± 0.42	26	116.01 ± 26.04
CPA-2F (g23000)	45 – 60	5.0000 ± 0.0005	2.741 ± 0.065	-3.5 ± 0.8	67.4	1.96 ± 1.05	25	115.07 ± 67.80
CPA-3F (g29582)	60 – 75	5.0013 ± 0.0005	4.117 ± 0.038	-14.6 ± 0.7	92.8	5.89 ± 0.41[d]	52	106.93 ± 9.64
CPA-4F (g27971)	75 – 90	5.0015 ± 0.0007	3.650 ± 0.041	-5.1 ± 0.6	74.8	6.07 ± 1.65	60	80.35 ± 24.25
CPA-5F (g27970)	90 – 105	5.0024 ± 0.0004	3.661 ± 0.052	-7.3 ± 0.8	73.3	5.89 ± 0.41[d]	59	81.91 ± 11.57
CPA-6F (g27969)	105 – 120	5.0004 ± 0.0040	3.424 ± 0.040	-7.6 ± 0.7	72.9	5.89 ± 0.41[d]	63	68.79 ± 8.39
CPA-7F (g29573)	120 – 135	4.9830 ± 0.0010	3.394 ± 0.037	-9.8 ± 0.8	79.7	5.89 ± 0.41[d]	64	66.70 ± 7.78
CPA-8F (g22999)	135 – 150	5.0013 ± 0.0005	1.648 ± 0.050	-1.1 ± 0.7	64.6	2.46 ± 2.11	54	41.04 ± 35.57
CPA-14P (g29566)	225 – 240	5.0048 ± 0.0005	2.279 ± 0.029	-8.4 ± 0.6	57.6	5.89 ± 0.41[d]	98	2.21 ± 13.00
Inchie Farm depth-profile[f]								
LM01F (g29583)	0 – 15	5.0038 ± 0.0010	3.040 ± 0.033	-10.7 ± 0.8	102.6	4.66 ± 0.46	48	84.14 ± 12.35
LM01P (g29584)	0 – 15	5.0041 ± 0.0006	3.167 ± 0.036	-15.6 ± 0.7	55.6	3.95 ± 0.48	55	76.79 ± 8.72
LM02F (g29576)	15 – 30	5.0033 ± 0.0008	2.974 ± 0.032	-9.0 ± 0.6	53.9	4.81 ± 1.17	60	63.48 ± 16.22
LM03F (g29575)	30 – 45	5.0029 ± 0.0005	3.232 ± 0.037	-9.5 ± 0.8	59.5	5.17 ± 0.72	59	71.33 ± 11.84
LM04F (g29574)	45 – 60	5.0040 ± 0.0005	2.513 ± 0.031	-9.7 ± 0.6	52.7	4.81 ± 0.46	72	36.83 ± 4.61
LM08F (g29572)	105 – 120	5.0037 ± 0.0006	2.386 ± 0.029	-11.7 ± 0.6	55.4	4.54 ± 0.50	73	34.08 ± 4.38

[a] Grains size fraction: F = 250 - 500 μm, M = 0.5 - 2 mm, P = 2 - 150 mm.

[b] All uncertainties reported at the 1σ level.

[c] Magnitude of blank used for correction expressed as % of the number of ^{14}C atoms in the sample.

[d] Long-term average blank.

[e] Latitude: 56.00936 (WGS84); Longitude: -4.47410 (WGS84); Elevation: 169 m a.s.l.

[f] Latitude: 56.17488 (WGS84); Longitude: -4.27385 (WGS84); Elevation: 36 m a.s.l.